AED R-3389
November 15, 1968

Second Quarterly Report: Action Of Lithium In Radiation-Hardened Silicon Solar Cells

Prepared for:
Jet Propulsion Laboratory
California Institute of Technology
Pasadena, California
In Response To:
Contract No. 952249

RCA | Defense Electronic Products
Astro Electronics Division | Princeton, New Jersey

CONTRACT NO. 952249

Action Of Lithium In Radiation-Hardened Silicon Solar Cells

Second Quarterly Report

Prepared for

Jet Propulsion Laboratory
California Institute of Technology
Pasadena, Calif.

By

G.J. Brucker, T.J. Faith, and A.G. Holmes-Siedle

Princeton, New Jersey

This work was performed for the Jet Propulsion Laboratory, California Institute of Technology, as sponsored by the National Aeronautics and Space Administration under Contract NAS7-100.

AED R-3389

Issued: November 15, 1968

NOTICE

This report contains information prepared by the Astro-Electronics Division of RCA under JPL subcontract. Its content is not necessarily endorsed by the Jet Propulsion Laboratory, California Institute of Technology, or the National Aeronautics and Space Administration.

PREFACE

This is the Second Quarterly Report on a program to study the "Action of Lithium in Radiation-Hardened Silicon Solar Cells." This report was prepared under Contract No. 952249 for Jet Propulsion Laboratory, Pasadena, California by the Astro-Electronics Division of RCA, Princeton, New Jersey. The period of performance covered by this report is from July 16 to October 15, 1968.

ABSTRACT

This is the Second Quarterly Report on a program to study and analyze the action of lithium in producing a recovery of radiation damage in silicon solar cells. This program has technical continuity with the work performed for NASA on Contract No. NAS5-10239. The eventual goal of this effort is to understand the recovery mechanism so that realistic predictions of solar-cell performance can be developed and optimum designs of lithium cells for space use can be specified.

The test vehicles being used for this work are (1) small-area solar-cell model devices, (2) a group of solar cells supplied by NASA on the above contract, (3) solar cells supplied by JPL, and (4) silicon bars, usually in the "Hall-bar" configuration. The source of particle irradiation being used is a 1-MeV electron beam produced by the RCA Laboratories Van de Graaff generator.

Continuing tests on GFE cells irradiated to fluences from 10^{14} to 10^{16} e/cm^2 indicate that to obtain good long-term stability in cells made from silicon of low oxygen content, lithium density should be made as low as is compatible with maximum cell recovery for the fluence applied to the cells. Cells with steep gradients of lithium density near the junction show gross lithium motion near the junction over $\approx$ 1 year. Cells of this type have redegraded as much as 35 percent eleven months after bombardment to 10^{14} e/cm^2. One unirradiated cell (out of 2 cells) of this type also showed $\approx$ 30 percent degradation in power. Redegradation in power output is due primarily to curve-shape changes and decreases in open-circuit voltage. Short-circuit current is, in general, constant during degradation.

Cells with smaller lithium-density gradient show better stability both before bombardment and after 10^{14} e/cm^2. Only one irradiated cell of nine and one unirradiated cell of nineteen have shown power (re) degradation beyond ±5-percent experimental uncertainty.

Pre-irradiation measurements made on 20 JPL-furnished Quartz-Crucible cells showed that a group of 10 cells with low-lithium-density gradient had tungsten efficiencies with an average of 10.9 percent; a second group of 10 cells with high-lithium gradient had tungsten efficiencies with an average of 7.5 percent.

Preliminary measurements on Float-Zone cells indicate that the lithium-diffusion constant in these cells increases with increasing distance from the junction.

Hall-coefficient and resistivity measurements have been used to investigate the crystal growth and irradiation-temperature dependence of the introduction rate and room-temperature annealing of carrier-removal defects in lithium-doped silicon. Initial resistivity of the Quartz-Crucible silicon was 30 ohm-cm and of the Float-Zone silicon was $\geq$1500 ohm-cm. The silicon was doped with lithium to a density of $2 \times 10^{16} cm^{-3}$. Irradiations were carried out with 1-MeV electrons at bombardment temperatures ranging from 79°K to 280°K. Specimens were annealed to 200°K thereby separating intrinsic and impurity defects. Introduction rates of carrier-removal defects were exponentially dependent on the reciprocal of temperature for both types of crystal, but the slopes and limiting temperature values differed. The slope of the carrier-removal rate versus reciprocal-temperature curve is 0.055 eV in Quartz-Crucible silicon and 0.09 eV in Float-Zone silicon. The temperature dependence was not consistent with a simple charge-state-dependent probability of interstitial-vacancy dissociation and impurity-vacancy trapping. Following the bombardments, the samples were allowed to warm up to room temperature (297°K). Spontaneous changes in carrier density and mobility occurred at room temperature in both types of silicon. Carrier densities measured at or near-room temperature decreased in Quartz-Crucible silicon and increased in Float-Zone silicon. Crucible-silicon samples annealed to 373°K for 10 minutes exhibited complete recovery of mobility. Complete recovery of mobility in Float-Zone silicon took place in an annealing time $\leq$17 hours at room temperature. The time constant of the annealing kinetics at room temperature is consistent with the smaller lithium-diffusion constant observed in oxygen-rich silicon compared to the free-lithium diffusion constant in oxygen-lean silicon. The mechanism of room-temperature annealing is attributed to neutralization of carrier-removal defects by lithium interaction in Quartz-Crucible silicon, and by both lithium interaction and defect dissociation in Float-Zone silicon. The LiO-V defect is tightly bound compared to the oxygen-free Li-V defect. Results suggest that a lithium-oxygen-vacancy complex is produced by radiation in Quartz-Crucible silicon and a lithium-vacancy complex in Float-Zone silicon.

TABLE OF CONTENTS

LIST OF ILLUSTRATIONS

LIST OF ILLUSTRATIONS (Cont'd)

Appendix Page

LIST OF ILLUSTRATIONS (Cont'd)

LIST OF TABLES

SECTION I

INTRODUCTION

A. GENERAL

It has been shown that at room temperature electron, proton, and neutron-irradiated silicon solar cells spontaneously recover their electrical outputs following irradiation (Reference 1). Initially, the loss of electrical output is due to degradation of minority-carrier lifetime. The mobile lithium ion moves toward and combines with a defect-impurity complex, thereby changing its electrical properties. In solar cells, the interaction of lithium with radiation-induced defects produces a defect complex which appears to have little or no effect on the minority-carrier lifetime.

The contract effort reported here represents an experimental investigation of the physical properties of lithium-containing p-on-n silicon solar-cells and of the processes that occur in these devices before and after irradiation. Its objectives are to identify the parameters which affect cell radiation recovery and long-term stability characteristics and to generate information which will lead to the optimization of these parameters. The eventual goal is to exploit this phenomenon for adaptation to the production of solar cells for the space environment. In this direction, it is anticipated that (1) realistic predictions of lithium-cell performance can ultimately be developed, and (2) optimum designs of lithium cells for space use can then be specified.

B. TECHNICAL APPROACH

Stated briefly, the approach to the objectives involves the testing of bulk samples as well as government furnished equipment (GFE)[1] and JPL-furnished[2] solar cells and in-house fabricated test diodes[3]. Experiments on bulk samples include Hall and

---

[1] Government Furnished Equipment under Contract No. NAS5-10239.

[2] Lithium-diffused cells delivered by JPL to RCA for evaluation as part of this contract effort.

[3] Test vehicles, similar to solar cells in all but photovoltaic response, fabricated to be compatible with experiments which appear particularly promising in terms of information yield as well as the experiments which are regularly performed in the course of the work. These test vehicles include both lithium-diffused and non-lithium-diffused diodes.

resistivity measurements taken as functions of (1) 1-MeV electron fluence, (2) sample temperatures during irradiation, and (3) isochronal anneals. Correlations of the results of these tests will be made wherever possible with the results of measurements on solar-cells and test-diodes. These measurements will include minority-carrier diffusion length versus (1) fluence, (2) temperature, and (3) annealing schedule; photovoltaic I-V characteristics; and reverse-bias capacitance measurements. In addition, stability tests are being continued on test-diodes and solar cells with post-irradiation histories dating back as far as December 1966.[1]

C. SUMMARY OF PRECEDING WORK (Late 1967 to Mid 1968)

For purposes of continuity, a brief history is given here of the recent work performed on the predecessor contract (Reference 2). This history will also provide the reader with a better understanding of the current technical approach, its problems, and its objectives.

In the work of the past year, in addition to continuing and extending a series of long-term stability tests on GFE[1] cells to in-house fabricated test-diodes[3] and to a second group of GFE[1] cells, extensive measurements of cell capacitance were made over a wide range of reverse biases. These measurements, which yield donor-density vs. distance from the junction, revealed large lithium-density gradients ($\sim 10^{19}$ cm^{-4}) near the junction and extending ($\geq 10\,\mu$m) from the junction. This gradient sets up a large internal electric field (>100 V/cm near the junction edge) thereby creating a field-aided diffusion situation for minority-carriers. This effect invalidates the concept of diffusion length for small lifetimes, i.e., where the electric-field effect is significant over a large fraction of the current-collection volume. This is the case after irradiation to fluences of the order 10^{15} to 10^{16} MeV/cm^2, making application of Waite's theory (Reference 3) very difficult. Accordingly, in the past year, some kinetic studies of damage recovery were made at lower fluences in the range 10^{13} to 10^{14} e/cm^2. Waite's theory, which reduces to a first-order kinetic equation at these fluences, was shown to describe the experimental recovery curves adequately for a large number of cells. These cells and cells irradiated to $\sim 10^{15}$ e/cm^2, as well as unirradiated cells, have since been undergoing long-term monitoring of their characteristics for stability of (1) minority-carrier diffusion length, and (2) photovoltaic I-V characteristics. These stability tests have continued as part of the present contract and they will be continued throughout the duration of this effort. The cumulative results through the end of this reporting period are presented and discussed in Section II of this report.

In the past year, the first known use was made of capacitance techniques for direct measurement of the lithium-diffusion constant in a solar cell (Reference 4). Results obtained by using this technique have indicated the possibility that the lithium-diffusion constant at the edge of the junction, where the measurements are made, is frequently

lower than that in the bulk of the current-collection volume. To clarify this question, which will have significant consequences in the understanding of cell stability, an attempt is being made to probe further into the base region of the cell by use of the capacitance method. The theoretical basis for the extension of such measurements is outlined in Section IV of the First Quarterly Report (Reference 5).

In addition to the fabrication of many test-diodes, the effort in the past year was directed toward modifying an existing apparatus for Hall measurements at liquid nitrogen temperature and toward the fabrication, lithium diffusion, and contacting of appropriate Hall samples. The purpose of these continuing measurements is to obtain information on the defect formation and annealing processes occurring in the lithium cell and the band-gap energy levels for defect structures occurring in these processes. Actual Hall measurements were started toward the end of Contract NAS5-10239 (Reference 2). These measurements were continued as part of the present contract effort and current results are given and discussed in Section V and Appendix I. This work was planned to be closely coordinated with the studies of the annealing of minority-carrier damage in experimental cells made from similar material. Correlation of data will be sought through the results of these sets of measurements. As a part of the measurements effort, a cold-finger apparatus has been constructed to enable cell (and test-diode) measurements to be made at temperatures as low as liquid-nitrogen.

SECTION II

STABILITY OF GFE CELLS

A. GENERAL

A large group of lithium-containing p/n silicon solar cells furnished under Contract No. NAS5-10239 (Reference 2) were irradiated by 1-MeV electrons. Measurements of cell parameters were made, including photovoltaic I-V characteristics under illumination by a filtered tungsten source at 100 mW/cm^2 and minority-carrier diffusion length (Reference 6) (based on the electron-voltaic method), both before irradiation and at periodic intervals after irradiation, continuing into the present reporting period. From the results of these and pre-irradiation capacitance measurements, information has been obtained on the stability of lithium-containing cells over a wide range of cell parameters, for electron fluences ranging from 10^{14} to 10^{16} e/cm^2. The duration of these tests ranges from 7 to 19 months. In addition to the experiments on irradiated cells, stability tests have been made on unirradiated cells for a period of eleven months. The cells in all the tests, both irradiated and unirradiated, were stored at room temperature, under fluorescent illumination under open-circuit conditions except for brief intervals (~hours) when photovoltaic, electron-voltaic, or reverse-bias capacitance measurements were being made. To date, the long-term reproducibility of the photovoltaic measurements from short-circuit current measurements is ±5 percent; the results of the diffusion-length measurements include an uncertainty of ±10 percent.

B. CELLS IRRADIATED TO 10^{16} e/cm^2 IN FEBRUARY AND MARCH 1967

During February and March 1967, a large number of GFE cells were irradiated to 10^{16} e/cm^2 at a flux rate of approximately 3 x 10^{15} $e/cm^2/hr$. These cells were manufactured by Texas Instruments, Inc., (Reference 7a) and Heliotek Division of Textron Electronics (Reference 7b). Periodic measurements of diffusion lengths and photo-response characteristics have been made on seventeen cells with varying phosphorus-background densities, growth methods, and lithium densities.

Table I lists values of phosphorous background density, ρ_0, and measured values of short-circuit current, J, and maximum power, P. Readings made before bombardment and approximately one hour, four days, three months, eight months, one year, 16 months, and 19 months after bombardment are included. The last readings were taken during the second quarterly reporting period. The pre-irradiation values of

TABLE I

STABILITY OF GFE CELLS IRRADIATED TO 10^{16} e/cm^2 IN FEBRUARY-MARCH 1967

Sample No.	ρ_o (in Ω-cm) and Growth Method	Initial Measurement (December 1966)		Post-Irradiation Measurements													
				1 Hour		4 Days		June 1967		November 1967		February 1968		July 1968		October 1968	
		J_o	P_o	J	P	J	P	J	P	J	P	J	P	J	P	J	P
Group 1 (<2 x 10^{15} cm^{-3})																	
TI 167	20 FZ	30.8	10.8	10.8	2.3	10.9	2.2	12.9	3.0	14.5	2.9	15.4	3.2	15.1	3.2	16.0	3.3
He 342	100 FZ	29.6	-	-	-	-	-	18.3	-	19.6	3.3	21.5	4.1	21.0	3.5	21.1	3.6
TI 63	20 FZ	29.6	10.4	9.5	2.0	11.2	2.1	15.7	3.4	17.6	3.9	19.3	4.5	19.3	4.6	20.0	4.8
TI 171	20 FZ	28.5	6.3	9.4	1.6	11.6	1.8	16.2	2.8	18.7	3.7	20.6	4.3	20.6	4.5	21.3	4.6
He 341	100 FZ	28.5	-	-	-	-	-	21.0	-	20.4	2.6	22.0	3.3	20.0	2.4	20.0	2.4
He 340	100 FZ	28.6	-	-	-	-	-	21.2	-	21.2	2.9	22.9	3.8	21.5	3.0	20.6	2.7
Group (2 to 5 x 10^{15} cm^{-3})																	
TI 112	20 QC	28.0	10.5	9.5	2.5	10.2	2.7	17.4	4.0	19.7	4.9	20.6	5.6	20.7	5.9	20.8	6.0
TI 113	20 QC	27.5	9.9	9.2	2.5	9.8	2.7	16.8	-	19.0	5.2	20.2	5.8	19.7	5.6	19.8	5.6
TI 168	20 FZ	28.8	11.2	9.9	2.5	13.5	3.3	16.7	4.0	17.6	4.4	18.6	4.8	18.0	4.6	18.7	4.9
TI 42	20 FZ	28.6	9.2	8.3	2.0	12.2	3.0	15.1	3.9	16.3	4.2	17.2	4.6	16.2	4.3	17.4	4.8
TI 161	20 FZ	27.2	10.8	8.9	2.6	17.1	5.1	17.4	5.3	17.4	5.5	18.2	5.8	17.1	5.4	18.0	5.8
Group 3 (7 to 10 x 10^{15} cm^{-3})																	
TI 128	20 L	28.5	10.8	9.1	2.5	16.7	5.0	16.0	4.9	15.7	3.4	16.2	3.6	15.4	4.0	16.4	3.9
TI 127	20 L	30.2	10.2	9.4	2.6	17.8	5.2	16.9	4.9	15.3	3.0	13.8	2.7	14.7	2.9	15.8	3.1
TI 132	20 L	29.8	-	10.7	1.5	16.2	4.8	15.2	4.1	15.8	4.0	16.2	4.1	15.1	3.7	16.2	4.0
TI 166	20 FZ	25.2	8.7	9.6	2.5	15.8	4.5	14.8	4.2	15.1	4.1	15.5	4.1	14.9	3.9	15.5	4.1
Group 4 (Phosphorus Doped)																	
He 248P	1000 FZ	24.8	8.4	16.6	3.8	22.3	6.1	22.5	5.0	22.2	6.3	23.5	7.0	23.0	6.7	23.8	6.5
He 249P	1000 FZ	24.2	8.4	13.2	3.5	20.6	5.7	23.7	6.3	22.2	6.9	22.8	7.4	22.2	7.3	22.7	7.3

NOTES: 1. J is measured in mA/cm^2
2. P is measured in mW/cm^2
3. FZ is Float Zone
4. QC is Quartz-Crucible
5. L is Lopex

lithium concentration, N_{Li}, measured at a distance of ≈ 1 μm from the junction by means of reverse-bias capacitance measurements (Reference 8), were found in early work under Contract NAS5-10239 (Reference 9). Table I also lists the performance history of these cells, which is given in four groups, as follows: The first group of six cells had initial lithium concentrations less than 2×10^{15} cm^{-3}; the second group of five cells had concentrations between 2 and 5×10^{15} cm^{-3}; the third group of four cells had concentrations between 7 and 10×10^{15} cm^{-3}. A fourth group of two cells, He 248P and He 249P, represent a special group of cells with a diffused heavily-doped phosphorus region near the junction.

The six cells of Group 1, although they have recovered to some extent, all have power levels below the ≈ 5.3 mW/cm^2 previously reported (Reference 10) for 10 Ω-cm n/p cells with initial power of ≈ 1.3 mW/cm^2 after a fluence of 10^{16} - 1 MeV electrons/cm^2. (Reference 10 is chosen for comparison with the data reported herein, rather than, e.g., the more recent Reference 11, due to the similarity in illumination conditions in Reference 10 and the present work, i.e., 100 mW/cm^2 filtered tungsten light.

The three Heliotek cells of Group 1 (He 340, 341 and 342), which were made from high-resistivity (100 Ω-cm) starting material, showed good recovery of minority-carrier lifetime, as seen from both diffusion-length and short-circuit current measurements. As of July 1968, He 341 had the highest diffusion length (25 μm) of the cells in Group 1; cells He 340 and 342 each had a 20 μm diffusion length. From Table I it is seen that these three cells also have high values of short-circuit current, J, relative to the other cells. In spite of this, they have three of the five lowest values of P (maximum power) of all the cells listed in Table I. The reason for these low powers is the very low filling factor, $f = P/JV_{OC} \lesssim 0.4$, found in the photo-response curves of these cells. This low filling factor is attributed to the high-resistivity starting material, which, together with the high-bombardment fluence, results in a low post-irradiation donor concentration. This could lead to problems in series resistance at the base contact or in parts of the body of the cell where lithium was heavily depleted.

Cell TI 167, which had the lowest lithium density (near the junction) of all the cells in Table I, recovered to ~ 3 mW/cm^2 at which power it has remained essentially constant since June 1967. It is thought that this cell has exhausted its free lithium supply near the junction thereby excluding the possibility of further room-temperature recovery. Seven TI cells with lower lithium density than cell TI 167 were dropped from this test soon after irradiation (Reference 9) when they displayed a very high series resistance together with a double junction. The photo-response of cell TI 167 indicates a high series resistance ($f = 0.5$) and also a significant shunt leakage of $\approx 80\Omega$.

The other two cells of Group 1, TI 63 and 171 continued to show significant recovery up to eleven months after irradiation. Over the past eight months the cells have remained essentially stable with a slight trend toward further recovery. As of the

latest reading TI 63 has the highest power of Group 1 cells, 4.8 mW/cm^2. Both of these cells have low filling factors; f $\approx$0.6 in TI 63, and $\approx$0.5, in TI 171. The shunt resistance in both cells is $\approx 200\,\Omega$. The filling factors in the (ρ_o = 20 Ω-cm) TI cells were, however, significantly higher than those in the (ρ_o = 100 Ω-cm) He cells, suggesting that problems such as series resistance can be adequately dealt with by judicious choice of silicon growth method, initial silicon resistivity, and lithium-doping level.

The cells of Group 2 had initial lithium densities, N_{L1} at $\approx$ 1 μm from the junction ranging from 2 to 5 x 10^{15} cm^{-3}. The common characteristic of the five Group 2 cells, together with He 248P and He 249P (1000 Ω-cm FZ) which will also be discussed now, is a recovered power level either close to or greater than the 5.3 mW/cm^2 of the 10 Ω-cm n/p cells of Reference 10. Figure 1 gives the maximum power, P, as a function of time, in days, after bombardment. The cells fall into three categories: (a) 20 Ω-cm Quartz-Crucible (QC) cells, TI 112 and 113, (b) 20 Ω-cm Float-Zone (FZ) cells, TI 42, 161 and 168, and (c) 1000 Ω-cm FZ cells with heavily doped (diffused) phosphorus layer near the junction, He 248P and 249P. No lithium-density data near the junction was obtainable on these last two cells due to the high phosphorus background.

The curves for the average values for categories (a), (b) and (c) are represented in Figure 1 by broken, solid, and dotted lines, respectively. It is seen that the 20 Ω-cm FZ and phosphorus-layer (b and c) cells recover rapidly over a period of several days then undergo an additional but very slow recovery for approximately one year. This slow long-term recovery in FZ cells could be explained in two different ways: first, the rapid initial flow of lithium to defects could cause local depletion of lithium near the junction, leaving some recombination centers after the initial fast recovery unsatisfied in their demand for lithium. Lithium would have to diffuse across large distances to satisfy these centers. A second possible explanation is that, over the long-term, recovery has to compete with some redegradation mechanism, i.e., recovery and redegradation mechanisms may be occurring simultaneously. Post-recovery redegradation of performance in lithium-doped cells has been observed here (e.g., Group 3 of the cells in Table I) and elsewhere (References 12 and 13) and its cause, although not well understood, has been suggested (Reference 14) to be the precipitation of lithium from the supersaturated solution that exists in the lithium-doped p/n silicon cell. (The solubility of lithium at room temperature in n-type silicon is $\sim 10^{13}$ cm^{-3}.) The precipitation of lithium in silicon is very much dependent on the heat-treatment history of the silicon after lithium doping (Reference 15) as well as on the initial lithium-doping level and silicon growth method (Reference 16). In any case, in the seven-month period since the end of the first year after bombardment these cells' power outputs have remained constant within experimental uncertainty, as have the other photovoltaic parameters, V_{oc} and J.

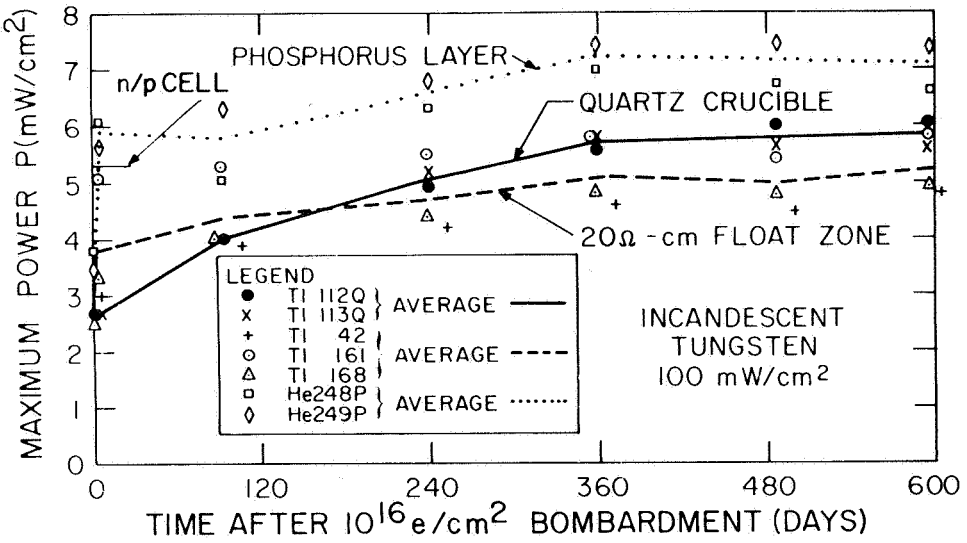

Figure 1. Annealing and Stability of Two Quartz-Crucible Cells, 20 Ω-cm Float-Zone Cells, and Two 1000 Ω-cm Float-Zone Cells With Diffused Phosphorus Layer After Bombardment By 1-MeV Electron to 10^{16} e/cm^2

Thus, if any redegradation has taken place, it has been counterbalanced by additional recovery. In this regard it is interesting to note that a slight increase in minority-carrier diffusion length has been observed during these last seven months. Thus the minority-carrier lifetime in the n-type base region is still slowly increasing, suggesting a small additional recovery.

In contract to the FZ cells, the QC cells recovered much more slowly at first due to the lowering of the effective lithium-diffusion constant caused by $(LiO)^+$ complexing (Reference 16), but continued to recover at a significant rate over the span of a year. At approximately a year after irradiation the power became stabilized (as did J and V_{oc}). The average powers for each category as of the latest readings were: (a) 5.8 mW/cm^2 for the QC cells, (b) 5.2 mW/cm^2 for the 20 Ω-cm FZ cells, and (c) 6.9 mW/cm^2 for the phosphorus-layer cells. The present (Oct. 1968) series resistance in the Group 2 cells has been compared with that in the initial measurements made before bombardment. The knees of the October 1968 I-V curves for the QC (category a) cells are sharper than the initial curves indicating that little, if any, series-resistance increase has occurred since the initial measurements. Similar comparisons on the 20 Ω-cm FZ cells (category b) show on the average a slight increase in series resistance. In the case of TI 161, the initial and translated October 1968 curves coincide exactly at the knee. In TI 168, the knee of the October 1968 curve being slightly below that of the initial curve ($\Delta V \approx 0.012$ volt, $\Delta J \approx 0.8$ mA/cm^2 near maximum power point). In the case of TI 42 the knee of the October 1968 curve is significantly sharper than that of the initial curve, which itself indicated a high series resistance. The initial curves for He 248P and 249P (category c) were too blurred to make a direct comparison of curve shapes. Comparison of filling factors (using data

of Reference 9) gives (an already low) f = 0.64 initially for both cells and f = 0.64 and 0.55 for He 249P and He 248P, respectively, as of October 1968. Thus, a filling factor decrease has occurred in the He 248P. It is not clear whether this decrease occurred during or after irradiation.

The shunt resistances of TI 42 and TI 168 were $\sim 200\,\Omega$ as of October 1968. All other Group 2 cells had shunt resistances greater than $500\,\Omega$.

It should be mentioned that of category (b) TI 161 with lithium density of 5×10^{15} cm^{-3} at $\approx 1\ \mu m$ from the junction recovered to the n/p level of 5.3 mW/cm^2 within three months after bombardment. This is significant since the radiation fluence of 10^{16} e/cm^2 of 1 MeV electrons is the equivalent of several years' dose in a particularly high-radiation Earth orbit. Cells TI 42 and 168, more lightly-lithium doped at $\approx 2 \times 10^{15}$ cm^{-3}, show slower recovery and stabilize at powers slightly below the n/p value (see Table I).

Cells He 248P and 249P have displayed particularly good behavior after irradiation. Though pre-irradiation power values (8.4 mW/cm^2 in each cell) were low, the resistance of the cells to irradiation was high, as seen from the values one hour after bombardment. Recovery continued steadily with time. As of the latest reading, approximately nineteen months after bombardment, the cells had values of 6.5 and 7.3 mW/cm^2 for P_{max} (i.e., ≈ 30 percent above the value for 10 Ω-cm n/p cells after bombardment to 10^{16} e/cm^2).

All four of the Group 3 cells in Table I (i.e., those with lithium density $\approx 1\ \mu m$ from the junction $> 7 \times 10^{15}$ cm^{-3}) showed significant redegradation between the fourth day after bombardment (March 10, 1967) and the 240th day (November 1967). In cell TI 127 this redegradation continued between the 240th and the 360th day to the extent that the value of P on the 360th day approximated that obtained one hour after bombardment. The value of P for the other Group 3 cells has remained constant within experimental error since the 240th day. It is noted that three of the four cells in Group 3 were Lopex* cells and that the cell suffering the least severe degradation was cell TI 166, the Float-Zone cell. The number of cells in this test is too small, however, to make any firm judgements on the relative merits of Lopex and Float-Zone cells. Since November 1967 the cells have stabilized. Averaging over the four cells of Group 3, the initial (pre-irradiation) power was $\overline{P}_o = 9.9$ mW/cm^2, that one hour after bombardment was 2.3 mW/cm^2, that at approximately maximum recovery four days after bombardment was 4.9 mW/cm^2 and that as of the October 1968 reading, 19 months after bombardment, was 3.8 mW/cm^2. Thus, on the average, these heavily lithium-doped cells did recover to a power slightly below the 5.3 mW/cm^2 level found for n/p cells, but subsequently redegraded, then stabilized at a power level approximately 25 percent below that at maximum recovery and 65 percent above the level one hour after

*Trademark of Texas Instruments, Inc.

bombardment. The values of J dropped slightly (less than 10 percent) in these cells during the redegradation process, however, the major factor in the redegradation was an apparent increase in series resistance as seen by changes in the shape of the I-V curves (Reference 17). The (already low) average filling factor, $\bar{f}$, for these cells was ≈ 0.65 initially. As of the most recent readings $\bar{f} \approx 0.50$. The shunt resistances were $\approx 70\ \Omega$ in TI 127 and TI 166, $\approx 250\ \Omega$ in TI 128, and $\approx 500\ \Omega$ in TI 132.

C. CELLS IRRADIATED TO $\approx 1.4 \times 10^{15}$ e/cm^2 ON NOVEMBER 1, 1967

On November 1, 1967 three TI cells made from 20 Ω-cm FZ silicon with lithium densities from 2 to 3 x 10^{15} cm^{-3} at $\approx 1\ \mu$m from the junction were irradiated to an incremental fluence of 10^{15} e/cm^2 in preparation for an injection level experiment reported previously (Reference 9). During the injection level tests an additional $\approx 0.4 \times 10^{15}$ e/cm^2 was applied for a fluence of $\approx 1.4 \times 10^{15}$ e/cm^2. These three cells, which have displayed similar behavior are represented in Figure 2. This figure gives plots of the averaged minority-carrier diffusion length (Reference 6), short-circuit current density, and maximum power for the three cells, each normalized to the pre-bombardment values of L_o, J_o, and P_o as functions of time (in hours) after bombardment. The power density scale is indicated on the right side of the figure together with the power density found for 10 Ω-cm n/p cells after irradiation to 1.4×10^{15} e/cm^2 (Reference 10). The error bars on the data points define the experimental uncertainty of the measurement. The first diffusion length was taken soon ($\sim$5 minutes) after bombardment to 10^{15} e/cm^2. The first $\overline{(J/J_o)}$ and $\overline{(P/P_o)}$ values, however, were taken 70 minutes after bombardment and therefore reflect the recovery during these 70 minutes (i.e., they are higher than the values immediately after bombardment). The initial, rising portions of the curves represent cell recovery. It is interesting to note that the time constant for recovery of the diffusion length, a parameter which is much more sensitive to electron irradiation than either the power or the short-circuit current, is approximately an order of magnitude shorter than that for recovery of power and short-circuit current. This suggests that the bulk lifetime is recovering at a more rapid rate than are the damage effects near the junction. The constant straight-line portions of the curves represent least square best fits (in this case a simple average) to a straight line with zero slope. It is seen that $\overline{(L/L_o)}$ has remained constant within experimental uncertainty (since recovery) for the eleven-month duration of the experiment. However, the normalized power, $\overline{(P/P_o)}$, suffered significant redegradation, from 0.59 to ≈ 0.50 between 5 and 8 months after bombardment, respectively. The normalized power has since stabilized over the present three-month reporting period at ≈ 0.52, a level of ≈ 6.8 mW/cm^2 which is significantly above the ≈ 6.0 mW/cm^2 for 10 Ω-cm n/p cells. Clearly, data over a longer period of time is required to establish whether these cells will remain stable at the present levels.

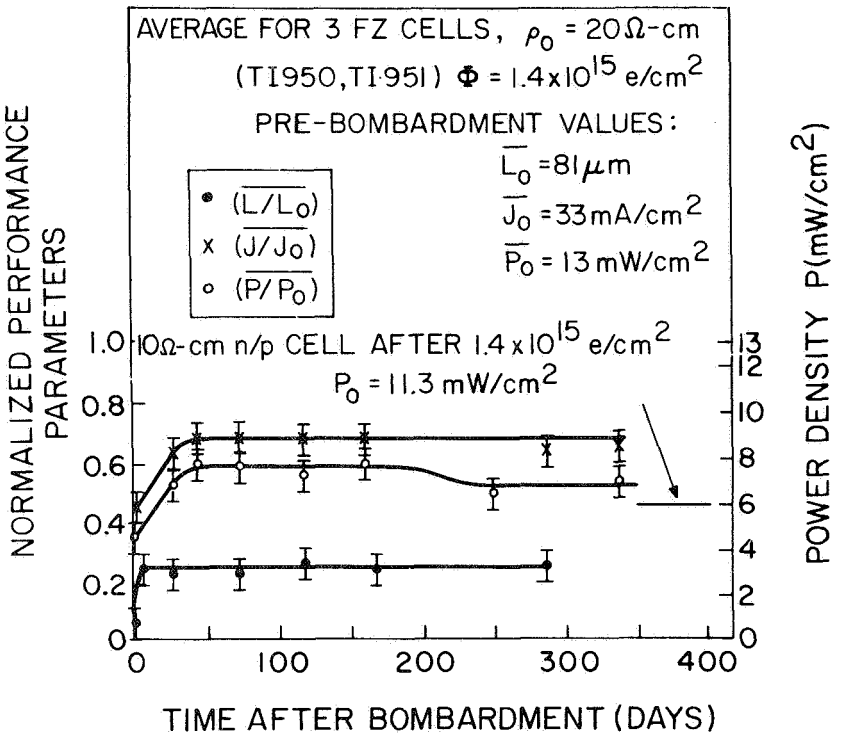

Figure 2. Stability of Performance Parameters in Three 20 Ω-cm Float-Zone Cells After Bombardment to 1.4 x 10^{15} e/cm^2

The stability of $\overline{(J/J_0)}$ is questionable. Although all the data points except the one at ≈250 days remain constant within experimental uncertainty, there is a noticeable downward trend after the 44-day reading. Decrease in open-circuit voltage, $\overline{V}_{oc}$, from 0.515 to 0.500, and filling factor, f from 0.67 to 0.65 were also encountered from the 44-day reading to the present reading. Evidently then, the redegradation here is due to the combined effect of three parameters: short-circuit current, open-circuit voltage, and possibly series resistance. The shunt resistance in each of these cells was well above 1000 Ω.

D. CELLS IRRADIATED TO 10^{14} e/cm^2 ON NOVEMBER 8, 1967

Four TI cells, three made from 200 Ω-cm Lopex silicon, one from 20 Ω-cm FZ silicon were irradiated to a fluence of 10^{14} e/cm^2 at a rate of ≈2 x 10^{13} e/cm^2/min. These cells had very high initial performance parameters, P_o and J_o, as shown in Table II, which also gives the values of P and J taken at six different times after irradiation, the latest values having been taken in the present reporting period. All of these cells have displayed significant post-recovery redegradation. However, the degree of redegradation varies significantly from cell to cell.

TABLE II

STABILITY OF GFE CELLS IRRADIATED TO 10^{14} e/cm^2 IN NOVEMBER 1967

Sample No.	ρ_o (Ω-cm) and Growth Method	October 1967		November 1967*		December 1967		March 1968		April 1968		July 1968		October 1968	
		J_o	P_o	J	P	J	P	J	P	J	P	J	P	J	P
TI 952	20 FZ	33.0	12.6	28.2	10.3	30.0	11.1	28.9	10.2	30.4	10.4	27.7	8.5	28.3	7.8
977	200 L	34.3	12.0	28.4	9.5	30.2	10.4	28.6	8.9	30.2	9.0	28.5	7.3	28.5	7.1
978	200 L	34.5	13.4	28.8	10.0	30.6	10.3	29.2	8.5	30.7	8.5	27.0	6.5	28.6	6.7
981	200 L	35.5	12.4	29.5	10.0	31.5	10.5	30.2	10.3	32.0	11.0	28.5	9.2	30.0	9.3

* values 8 days after bombardment.

TI977 and 978 both have suffered severe redegradation since ≈100 days after bombardment. This is clearly seen in Figure 3 which gives plots of L, J, P, and V, normalized to the pre-irradiation values, as functions of the time after irradiation. These values are the averages for TI 977 and 978 which have displayed similar behavior. The values of J, P, and V immediately after irradiation were not obtained because diffusion-length recovery experiments (Reference 4) were made (on all four cells) after irradiation. The diffusion length ≈5 minutes after bombardment was 0.16 of its original value. Recovery to 0.63 L_o occurred at room temperature in less than 2 hours. In the ensuing ≈ 240 days a decrease to 0.50 L_o has occurred. This represents a small fractional change (within the ±10 percent uncertainty in the diffusion length measurement) which would not be expected to significantly affect the photovoltaic parameters since the latter are insensitive to small minority-carrier lifetime changes (varying logarithmically with lifetime). This is verified by the stability of the normalized short-circuit current, J/J_o, shown in Figure 3. All short-circuit current values are constant after recovery within the (±5 percent) experimental uncertainty of the measurements. Nevertheless the output has suffered redegradation from 0.82 P_o at maximum recovery to 0.54 P_o as of the most recent measurement, a drop of ≈35 percent. In addition the open-circuit voltage has redegraded from 1.0 V_o to 0.82 V_o, a highly significant decrease.

Figure 4 shows the photovoltaic characteristics of TI 978 taken at three different times; (a) before bombardment, (b) at the time of maximum power after recovery, and (c) as of the latest reading, 331 days after bombardment. The shape of the curve taken 331 days after bombardment indicates a severe redegradation due to a ≈15% drop in filling factor in addition to the redegradation caused by the ≈20 percent drop in open-circuit voltage. By comparison, the decrease in short-circuit current is only 6 percent, i.e., within experimental uncertainty. Figure 4 clearly demonstrates that the stability of short-circuit current is not a valid criterion for lithium cell stability. A valid stability criterion is obtained only through examination of the entire photovoltaic response characteristic.

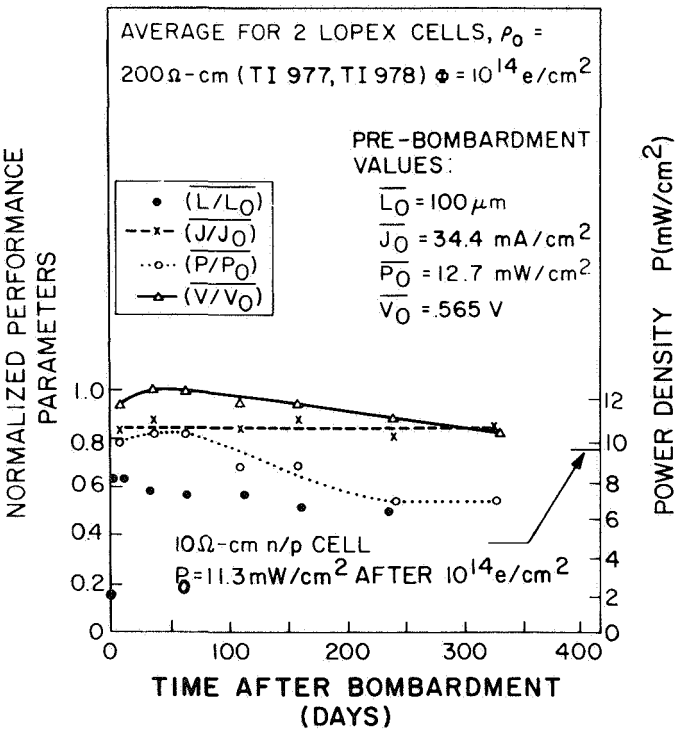

Figure 3. Stability of Performance Parameters in Two 200 Ω-cm Lopex Cells After Bombardment to 10^{14} e/cm^2

The other Lopex cell, TI 981, has suffered 11 percent redegradation. In addition to suffering less redegradation than TI 977 and 978 the stability time of TI 981 after recovery, i.e., $\gtrsim$ 160 days, is somewhat greater than that for TI 977 and 978, i.e., $\approx$100 days. The causes of redegradation, however, are the same, namely, a $\approx$6 percent decrease in open-circuit voltage and a change in filling factor from 0.63 after recovery to 0.59 after redegradation. It is noted that a 6 percent decrease in V is significant. This is due to the logarithmic variation in V with I_L, the light-generated current, which causes the experimental uncertainty to be less than that in J and P.

TI 952, the Float-Zone cell, irradiated to 10^{14} e/cm^2 displayed post-irradiation behavior similar to that of the Lopex cells just discussed. Power redegradation was from 0.88 P_0 to 0.62 P_0; open-circuit voltage from 0.570 to 0.521 V; filling factor from 0.66 to 0.53.

The power after recovery in these cells ranged from $\approx$5 to 12 percent above that found for 10 Ω-cm n/p cells (Reference 10) after 10^{14} e/cm^2. The powers after redegradation range from $\approx$2 to 22 percent below the n/p level.

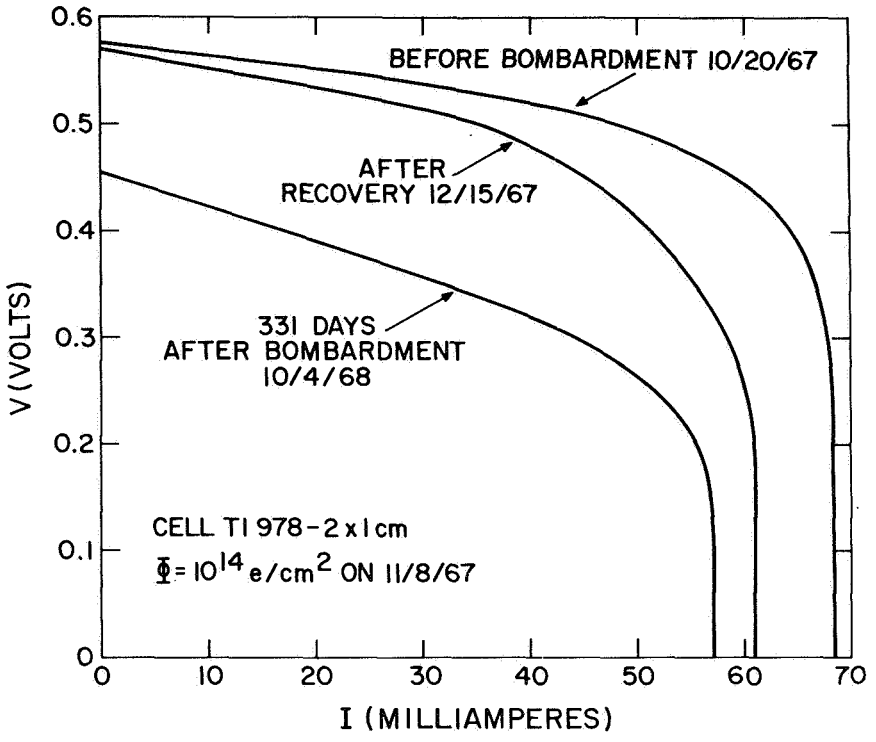

Figure 4. Comparison of Photovoltaic Characteristics of Lopex Cell TI 978 Before Bombardment, After Recovery Following Bombardment to 10^{14} e/cm^2, and After Redegradation

E. CELLS IRRADIATED TO 10^{14} e/cm^2 ON MARCH 12, 1968

A total of nine Heliotek cells were irradiated to 10^{14} e/cm^2 at a rate of $\approx 2 \times 10^{13}$ e/cm^2/min on March 12, 1968. Eight of these cells were made from 20 Ω-cm Float-Zone silicon, one from 20 Ω-cm Lopex silicon. The performance histories of these nine cells is given in Table III. The initial performance levels of the cells was somewhat below that of the TI cells discussed in the previous section. The post-recovery performance of the first two cells in Table III, He 651 and 670, has been erratic. We don't understand the reason for this, however, the most recent power readings are only ≈8 percent below the initial (pre-irradiation) powers.

The remaining seven cells are very similar to each other. All cells underwent the same lithium-diffusion cycle, namely, diffusion from the back surface for 60 minutes followed by a 90-minute redistribution, all done at 350° C (Reference 18). Their initial performance parameters were also similar and their post-irradiation properties have been reasonably similar. They will therefore be discussed as a group except where comments on individual cells are deemed appropriate.

TABLE III

STABILITY OF GFE CELLS IRRADIATED TO 10^{14} e/cm^2 IN MARCH 1968

Sample No.	ρ_o (Ω-cm) and Growth Method	November 1967		March 1968*		March 1968**		April 1968		July 1968		October 1968	
		J_o	P_o	J	P	J	P	J	P	J	P	J	P
He 651	20 FZ	26.3	9.8	27.2	10.3	23.9	8.9	27.4	10.2	23.4	6.8	25.7	9.1
670	20 L	27.7	10.8	28.6	10.6	24.7	9.5	28.1	6.6	25.6	8.9	26.6	10.0
798	20 FZ	27.6	10.4	28.6	11.1	23.4	8.5	28.5	10.8	26.3	9.8	27.3	10.1
810	20 FZ	28.9	10.0	28.9	10.0	24.1	8.1	28.9	10.2	26.9	9.2	27.7	9.5
879	20 FZ	30.1	11.9	30.9	12.3	25.0	9.2	31.0	12.0	29.1	10.9	29.4	11.1
881	20 FZ	29.6	11.2	30.4	10.1	25.5	8.4	30.3	9.5	28.2	9.4	28.7	8.4
882	20 FZ	29.6	11.4	30.5	11.9	25.1	9.0	30.5	11.6	28.5	10.6	28.8	10.6
884	20 FZ	30.2	10.8	31.2	11.3	25.1	8.6	30.9	11.1	28.9	10.4	29.0	10.1
885	20 FZ	28.9	10.9	29.8	11.3	24.6	8.8	30.0	11.3	28.2	10.5	28.3	10.3

*Before bombardment.
**≈ 40 minutes after bombardment.

Figure 5 gives performance histories as a function of time after bombardment averaged over the seven cells: He 798, 810, 879, 881, 882, 884, and 885. The pre-bombardment values of $\overline{P_o}$ = 11.1 mW/cm^2 and $\overline{J_o}$ = 30.0 mA/cm^2 were reasonably high.

The first post-bombardment value of $\overline{(L/L_o)}$, taken ≈5 minutes after bombardment, was 0.24. This is significantly higher than that averaged over the four TI cells, namely 0.15. The first values of $\overline{(J/J_o)}$ and $\overline{(P/P_o)}$ in Figure 5 were taken ≈40 minutes after bombardment. These normalized values are remarkably high, 0.87 and 0.78, respectively. This indicates a higher resistance to radiation damage than was found in the TI cells irradiated to 10^{14} e/cm^2, as would be expected given the higher initial performance of the TI cells. The next readings, taken 35 days after bombardment indicate practically complete recovery of photovoltaic response. The readings taken on this day, however, were approximately 5 percent higher on all cells than those taken on other days. It is felt, then, that the light intensity at the cells' surfaces was actually ≈105 mW/cm^2 and thus the true values of $\overline{(J/J_o)}$ and $\overline{(P/P_o)}$ should be ≈0.95 and ≈0.92, respectively, rather than the 1.0 and 0.97 readings shown in Figure 5. Subsequent readings gave $\overline{(J/J_o)}$ = 0.93, and $\overline{(P/P_o)}$ = 0.91 on the 119th day after bombardment; and $\overline{(J/J_o)}$ = 0.95 and $\overline{(P/P_o)}$ = 0.90 on the 206th day after bombardment. The photovoltaic characteristics of six of the seven cells of this group show no sensible redegradation or change in shape. One of the seven cells, He 881, did display a significant power redegradation. The series resistance of this cell after redegradation, as measured by the technique of Wolf and Rauschenbach (Reference 19), was ≈2.8Ω. Thus the redegradation was presumably due to a series resistance increase. The filling factor of He 881 decreased from 0.63 to 0.56, and the power from 9.4 to 8.4 mW/cm^2 during this time. The short-circuit current and open-circuit voltage remained constant during this time, thus the redegradation in this cell was due solely to an increase in the series resistance of the cell.

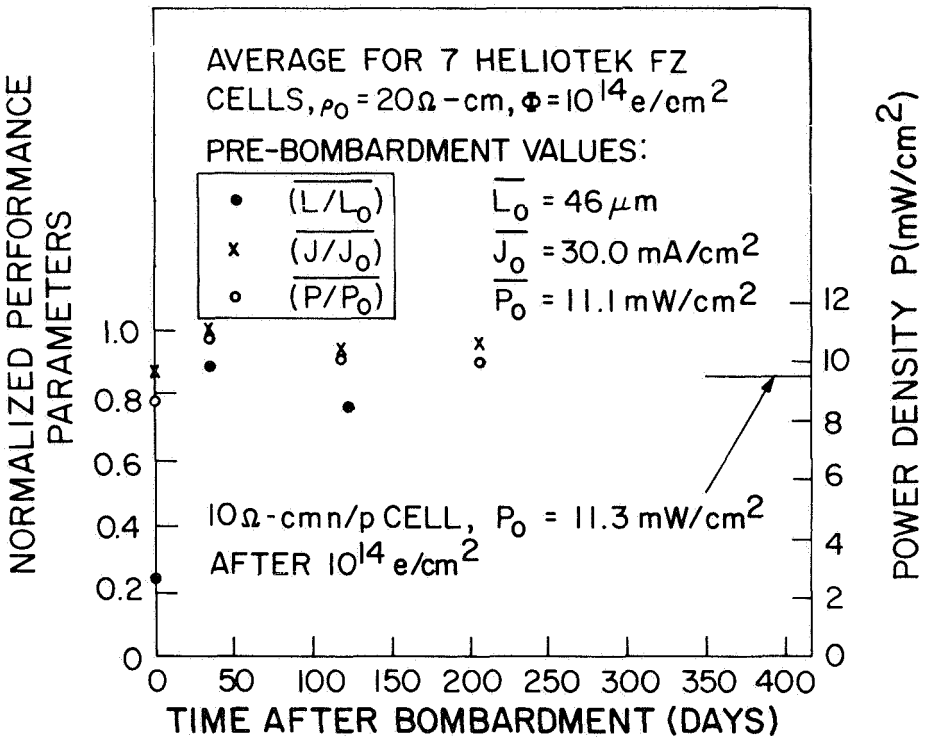

Figure 5. Stability of Performance Parameters in Seven 20 Ω-cm Float-Zone Cells After Bombardment to 10^{14} e/cm^2

Although the duration of the post-irradiation stability tests on these Heliotek cells has been shorter (206 days) than those on the Texas Instruments cells after 10^{14} e/cm^2 (331 days), sufficient data exists to indicate better long-term stability in the Heliotek cells. It should be stated that the initial values of N_{L1} in all the TI cells placed them in either Group I or II (see Section II-B), i.e., lithium densities less than 5 x 10^{15} cm^{-3}. The effect of lithium-density distribution on cell stability after various radiation levels will be discussed more thoroughly in Section II-G.

All of the cells irradiated to 10^{14} e/cm^2 had, as of October 1968, shunt resistances greater than 1000 Ω. Thus shunt leakage has not been a factor in cell performance.

F. UNIRRADIATED CELLS

Table IV presents a performance history for nineteen He cells and two TI cells covering approximately eleven months. The last readings were taken during the present reporting period. A negligibly small electron fluence was applied to each cell during minority-carrier diffusion-length measurements. This fluence is calculated to be less than 10^{10} e/cm^2.

It is seen from Table IV that of all the cells tested only He 867 and TI 979 have suffered degradation in power output. (The March power measurement on He 815 is considered in error, probably due to faulty contacts.) In He 867 the power degradation

TABLE IV.

PERFORMANCE HISTORY OF UNIRRADIATED CELLS

Sample No.	ρ_o and Growth Method	November 1967		March 1968		July 1968		October 1968	
		J_o (mA/cm^2)	P_o (mW/cm^2)	J (mA/cm^2)	P (mW/cm^2)	J (mA/cm^2)	P (mW/cm^2)	J (mA/cm^2)	P (mW/cm^2)
He 673	20 L	24.3	8.8	25.0	9.4	23.1	8.5	24.5	8.9
676	20 L	25.9	9.1	26.6	9.7	24.7	8.9	26.0	9.2
694	20 L	25.8	9.4	26.8	9.7	24.9	9.3	26.3	9.7
796	20 FZ	26.0	9.5	26.9	10.3	25.2	9.4	26.1	9.7
808	20 FZ	26.4	9.6	27.2	10.0	25.8	9.5	26.6	9.7
815	20 FZ	28.3	11.0	29.1	8.5	27.7	11.0	28.7	11.6
866	20 FZ	29.0	10.8	30.2	11.5	29.0	11.0	29.3	11.2
867	20 FZ	28.6	10.7	29.9	11.8	28.5	10.8	28.9	9.7
868	20 FZ	26.5	9.9	28.0	10.7	26.6	10.0	26.9	10.2
870	20 FZ	28.0	10.5	29.6	11.2	28.5	10.8	29.0	10.9
871	20 FZ	29.6	11.2	31.6	12.4	30.5	12.0	30.9	12.0
872	20 FZ	-	-	28.0	10.6	27.1	10.2	27.6	10.2
873	20 FZ	29.0	11.6	30.0	11.4	29.0	11.1	29.2	11.2
875	20 FZ	28.1	10.7	29.1	10.9	27.8	10.3	28.0	10.3
876	20 FZ	27.6	9.6	28.6	11.0	27.5	10.5	27.9	10.5
878	20 FZ	28.3	11.1	26.1	11.2	28.2	10.8	28.3	10.7
886	20 FZ	29.1	10.7	30.4	11.5	29.5	11.2	30.3	11.7
887	20 FZ	30.6	10.8	31.8	11.4	30.7	10.9	31.6	11.6
892	20 FZ	28.9	11.0	29.8	11.4	29.0	11.6	29.6	11.8
TI 976	200 L	32.0	12.1	33.8	12.9	32.5	11.8	33.2	12.8
979	200 L	32.4	11.8	34.3	11.0	33.2	8.4	34.1	8.3

Notes: 1. L is Lopex
2. FZ is Float Zone

amounted to ≈15 percent and occurred only after eight months. The main cause of the degradation was a series resistance increase, f decreasing from 0.79 in July 1968 to 0.65 in October 1968. In contrast, TI 979 showed significant degradation between 4 and 8 months after the first measurement and as of the latest measurement was ≈35 percent below the initial value obtained in November 1967. This 35 percent is the same as the amount of redegradation suffered by two similar TI cells (977 and 978) after irradiation to 10^{14} e/cm^2 in November 1967. In fact the changes in I-V characteristic in TI 979 are approximately the same as were the changes in I-V characteristic in TI 977 and 978 (Figure 4). A decrease in the open-circuit voltage TI 979 from 0.570 V to 0.510 V has occurred in addition to a severe drop in filling factor, f = 0.64 in November 1967 to f = 0.48 in October 1968. During the same time period the short-circuit current has remained constant within experimental uncertainty.

The initial values of N_{L1} in the unirradiated cells placed them in either group I or II (see Section II-B), i.e., lithium densities less than 5 x 10^{15} cm^{-3} at ≈ 1 μm from the junction. It will be seen in the discussion which follows that, while being a useful index of the effect of lithium on cell stability, the initial lithium density value taken from capacitance measurements about a single value of reverse bias, is not sufficient for the establishment of a cell-stability criterion.

G. DISCUSSION OF STABILITY RESULTS

Summarizing the results of the stability tests after various electron fluences, considering for the moment only FZ and Lopex cells:

(1) TI cells irradiated to 10^{16} e/cm^2 have not redegraded after recovery unless $N_{L1} > 5 \times 10^{15}$ cm^{-3}. Three He cells (He 340, 341, and 342 with $N_{L1} \lesssim 2 \times 10^{15}$ cm^{-3}) show spotty behavior. This is attributed to a very low donor density and consequent series-resistance increase.

(2) Three TI cells ($2 \times 10^{15} < N_{L1} < 3 \times 10^{15}$ cm^{-3}) have shown slight redegradation 11 months after bombardment to $\approx 1.4 \times 10^{15}$ e/cm^2.

(3) Four TI cells ($1.7 \times 10^{15} < N_{L1} < 3.5 \times 10^{15}$) showed significant redegradation $\sim$100 days after bombardment to 10^{14} e/cm^2. Approximately one year after bombardment three of these cells have redegraded to a power $\approx$35 percent below the maximum power achieved during recovery. On the other hand, only one of seven Heliotek cells has redegraded significantly $\sim$200 days after bombardment to 10^{14} e/cm^2. The lithium density, N_{L1}, in these cells ranged from 1.2 to 1.7×10^{15}. He 881 ($N_{L1} = 1.7 \times 10^{15}$ cm^{-3}) has redegraded 10 percent due to an increase in series resistance.

(4) Eighteen of nineteen unirradiated Heliotek cells ($1 \times 10^{15} < N_{L1} < 3.6 \times 10^{15}$ cm^{-3}) have been stable over an eleven-month period. The one cell which degraded was He 867 which had an initial value of $N_{L1} \approx 1.0 \times 10^{15}$ cm^{-3}. This cell degraded because of an increase in series resistance. Of the two unirradiated TI cells, TI 979, with $N_{L1} = 1.6 \times 10^{15}$ cm^{-3}, has degraded severely ($\approx$ 30 percent) while TI 976, $N_{L1} = 4.1 \times 10^{15}$ cm^{-3}, has remained stable.

In light of the above summary, considering only the TI cells for the moment, it is clear that for a given value of N_{L1}, the lower the fluence the more severe the redegradation. In addition, the higher the value of N_{L1} for a given fluence, the more severe the redegradation. The latter was seen to be the case for cells irradiated to 10^{16} e/cm^2. Figure 6 shows it to apply to the three Lopex cells irradiated to 10^{14} e/cm^2. Figure 6 presents plots of donor density versus distance from the junction for the three Lopex cells TI 977, 978, and 981. These plots were obtained from reverse-bias capacitance measurements (Reference 8) on the cells taken with a Boonton Model 74D capacitance bridge. As indicated in Figure 6 one set of plots was taken on October 23, 1967, before bombardment, and another on October 11, 1968, after redegradation. The cells are labelled on each plot; on the plots taken after redegradation the percents redegradation in V and P are also given. Figure 6 has many noteworthy features: (1) the very great increase in lithium density near the junction in each cell, (2) the cells with higher density have higher density gradients, (3) the percent redegradation increases with increasing cell density, and (4) the increase in density at a given distance from the cell junction over the period of $\sim$1 year is greater for the higher density cells. Thus redegradation in these cases correlates with large changes in lithium-donor profile adjacent to the junction. The significant slope of the redegraded curves near the voltage axis (see Figure 4) suggests a high series resistance in these cells. This could occur in the form of sheet resistance if enough lithium donors cross the junction to the p-skin to significantly compensate the boron acceptor. However, a recent 4-point probe measurement (Reference 20) on

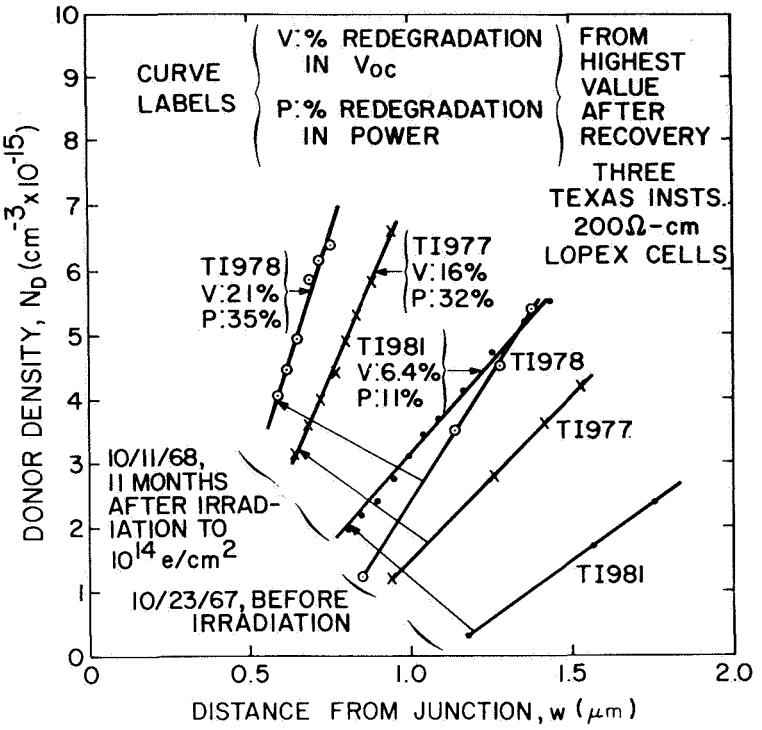

Figure 6. Comparison of Donor Density Profiles of Three Lopex Cells Before Bombardment and 11 Months After Bombardment to 10^{14} e/cm^2

the p-skin of TI 978 indicated very heavy ($\sim 10^{20}$ cm^{-3}) boron doping. In addition, in measurements of series resistance (Reference 19) on the TI cells showing redegradation, the values found were very low, e.g., TI 952, $R_S \approx 0.60\ \Omega$; TI 978, $R_S \approx 0.32\ \Omega$. The values were in fact somewhat lower than the average for the seven Heliotek cells bombarded to 10^{14} e/cm^2, namely $\approx 1.2\ \Omega$.

Thus a contradiction is evident. The redegraded (TI) cells display I-V characteristics suggesting large series resistance, however direct measurements give low values of series resistance. In addition, the decrease in open-circuit voltage in the same TI cells is puzzling. The shunt resistances in these cells is too high ($>1000\ \Omega$) to significantly effect the I-V characteristic. It must be said, then, that the photovoltaic response of these cells is not understood in terms of present solar cells equivalent circuits.

Both unirradiated TI cells display spontaneous increases in lithium concentration near the junction similar to those shown in Figure 6. However, as stated before only TI 979 degraded in output. Its series resistance was measured to be $\approx 0.68\ \Omega$. TI 976 which didn't degrade indicated a series resistance of $\approx 0.63\ \Omega$. It is not understood why TI 976 did not degrade.

The question also arises as to why the Heliotek cells, both those irradiated to 10^{14} e/cm^2 and those left unirradiated, have not (in most cases) redegraded (or degraded). A possible explanation for this is contained in Figure 7 which gives density profiles for two cells on two dates ~1 year apart. Both of the cells were fabricated from 20 Ω-cm FZ silicon and both were irradiated to 10^{14} e/cm^2. One of them, TI 952 started to redegrade ~100 days after bombardment and had redegraded ≈30 percent in power 331 days after bombardment. The other, He 810, had shown no sensible redegradation 206 days after bombardment. The initial (10/23/67 and 11/30/67, respectively) densities of the two cells at zero bias were equal within the ≈±5 percent experimental uncertainty of the measurement. That for TI 952 was 9.5 x 10^{14} cm^{-3} and that for He 810 was 9.0 x 10^{14} cm^{-3}. However, the similarity ends here. The slope, dN_D/dw, of the initial TI 952 profile was 3.0 x 10^{19} cm^{-4}, more than three times the 0.9 x 10^{19} cm^{-4} of He 810. The density profiles taken approximately eleven months later on October 11, 1968, show an even more striking contrast. TI 952 displayed a large increase in density near the junction as had the other TI cells. On the other hand, He 810 showed a slight decrease in density from the initial reading. In addition, whereas the density gradient in TI 952 was 7.0 x 10^{19} cm^{-4}, giving a density of 5.8 x 10^{15} cm^{-3} at a distance of 1.3 μm from the junction, the density gradient in He 890 decreased at ≈2 μm to 0.2 x 10^{19} cm^{-4}, a factor of 70 below that of TI 952. Thus, although the initial densities of the two cells at the edge of the

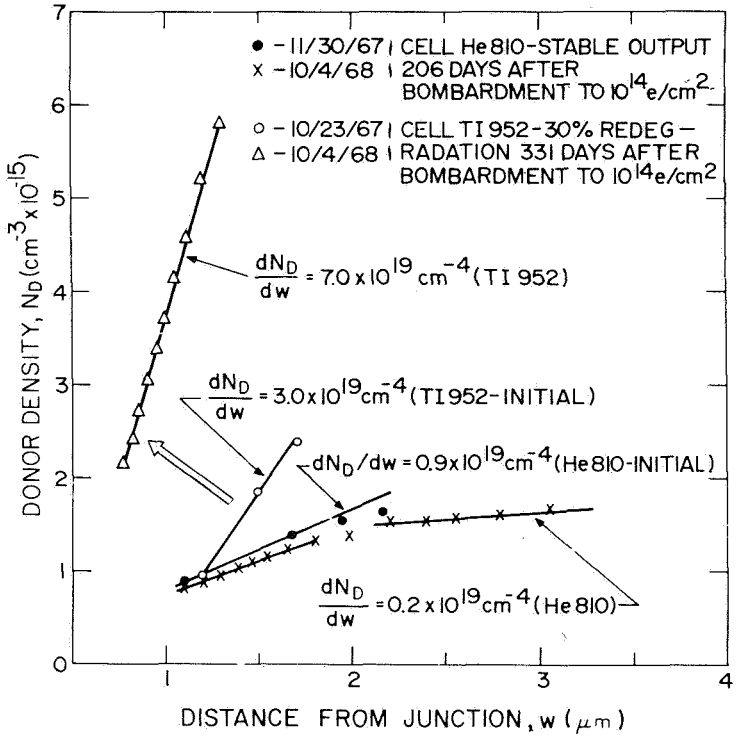

Figure 7. Comparison of Donor Density Profile Histories of a Cell Which Redegraded After Recovery From 10^{14} e/cm^2 and a Cell Which Maintains a Stable Output After Recovery From 10^{14} e/cm^2

depletion region were approximately equal, their density profiles and the subsequent behavior of these density profiles were enormously different. The behavior of He 810 was typical of all the Heliotek cells. From the above it is inferred that the lithium motion in the junction region in the Heliotek cells is much less than that in the TI cells. It is likely that this reduced motion is responsible for the better stability of the Heliotek cells.

SECTION III

CELLS FURNISHED BY JPL

A shipment of twenty lithium-containing Quartz-Crucible cells were received from JPL in August 1968. Ten of these cells were manufactured by Heliotek and ten cells by Centralabs. On September 6, 1968, initial measurements of photovoltaic response were made on these cells. Current-Voltage characteristics were obtained on a 139.6 mW/cm^2 tungsten illuminator using a Spectrolab Model D550 Electronic Load. In addition, measurements were made on a three-color filter wheel. Short-circuit current at air-mass zero I_o(AMO) was obtained from a computer program using the filter wheel data (Reference 21). Both the tungsten illuminator and the filter wheel have maintained 1-percent reproducibility over a period of years. Table V lists the initial short-circuit current densities, J_o, maximum power densities, P_o, open-circuit voltages, V_o, efficiencies, η_o, under tungsten illumination, and the short-circuit currents, I_o (AMO), from the filter wheel. The total cell area (2x1 cm^2) was used to calculate the current densities and power densities. The 10 Heliotek cells, with arsenic-doped starting resistivity of 100 to 200 Ω-cm, and diffused from a lithium paint-on source with diffusion time/temperature: 90 min/425° C, and redistribution time/temperature: 60 min/425° C, had an averaged efficiency of 7.45 percent. The 10 Centralabs cells, with arsenic-doped starting resistivity of 25 to 35 Ω-cm, and diffused from a lithium paint-on source with diffusion time/temperature: 5 min/450° C, and redistribution time/temperature: 40 min/450° C, had an averaged efficiency of 10.9 percent. Reverse-bias capacitance measurements (Reference 8) were made on all twenty cells. The resulting donor-density profiles for the most heavily doped (H1-7) and most lightly doped (H1-26) Heliotek cells and for the most heavily doped (C1-22) and most lightly doped (C1-28) Centralab cells are given in Figure 8. The density profiles of the Heliotek cells thus lie within the bounds defined by H1-7 and H1-26, and the Centralab cells within those defined by C1-22 and C1-28. Thus, the Heliotek cells are more heavily doped with lithium near the junction than are the Centralab cells.

A second batch of thirty QC cells, ten each from Centralab, Heliotek, and Texas Instruments, were received in September. They are currently undergoing initial measurements.

TABLE V

INITIAL PERFORMANCE PARAMETERS OF JPL-FURNISHED CELLS

Cell	J_o (mA/cm^2)	P_o (mW/cm^2)	V_o (V)	η_o (%)	I_o (AMO) (ma)
H1-6	25.3	9.6	0.546	6.85	56.4
H1-7	22.6	8.5	0.540	6.10	52.3
H1-8	25.3	9.7	0.559	6.95	55.1
H1-9	22.8	8.9	0.547	6.35	52.3
H1-10	26.8	10.5	0.566	7.50	58.3
H1-26	28.2	11.4	0.567	8.15	60.4
H1-27	28.1	11.6	0.569	8.30	60.5
H1-28	27.9	11.4	0.569	8.10	59.7
H1-29	27.6	11.1	0.571	7.95	59.0
H1-30	28.6	11.4	0.569	8.10	-
C1-21	35.2	15.4	0.601	11.0	67.8
C1-22	35.6	14.7	0.604	10.5	68.0
C1-23	34.7	15.2	0.598	10.8	66.9
C1-24	34.5	14.9	0.597	10.6	67.6
C1-25	36.0	15.8	0.604	11.2	69.9
C1-26	36.0	16.1	0.606	11.4	69.0
C1-27	35.8	15.8	0.602	11.2	70.0
C1-28	36.1	15.6	0.602	11.1	70.0
C1-29	35.4	15.0	0.599	10.7	69.5
C1-30	36.7	15.0	0.600	10.7	69.9

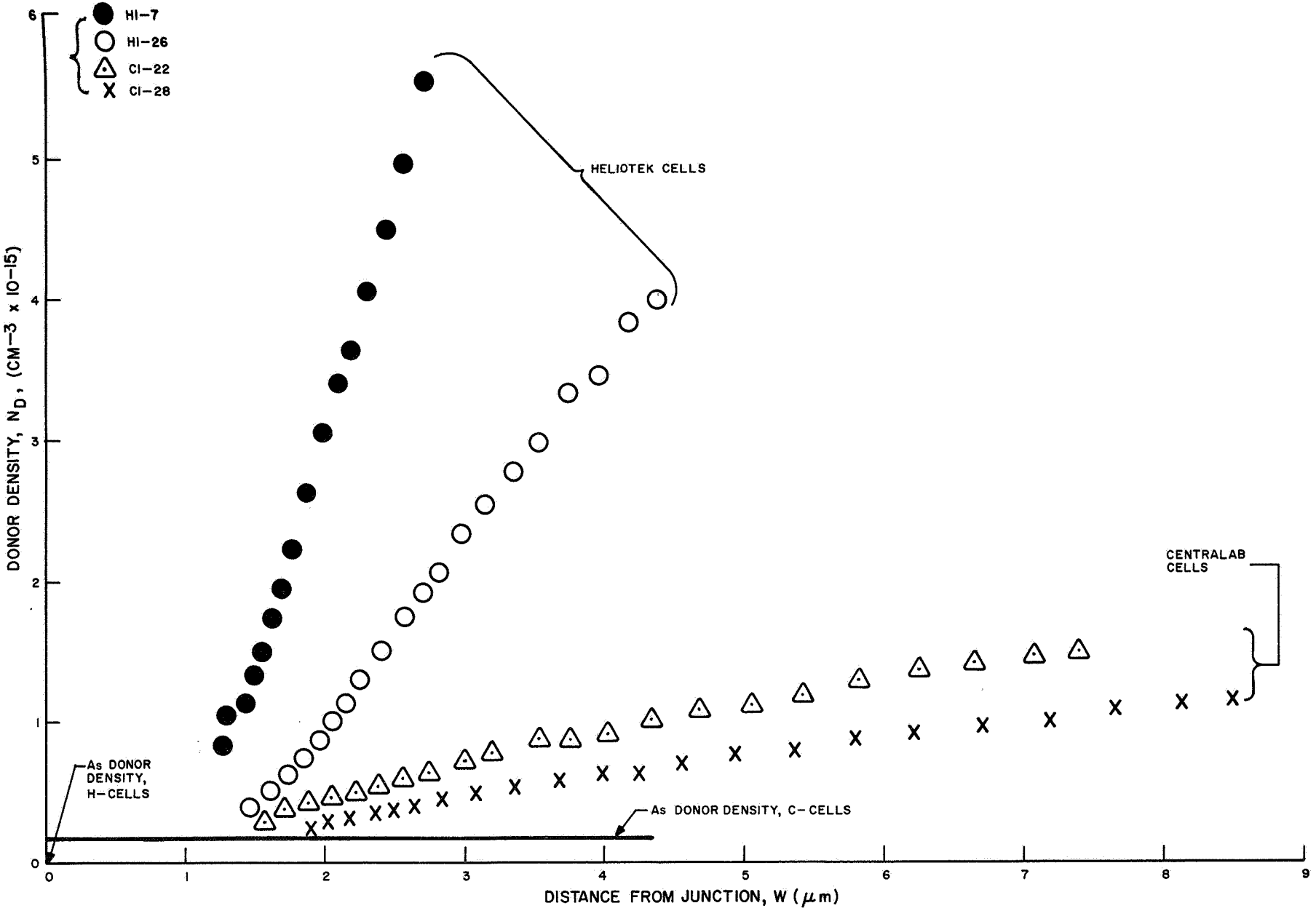

Figure 8. Comparison of Highest and Lowest Donor Density Profiles for Two Types of Lithium Cells Furnished by JPL in 1968

SECTION IV

MEASUREMENTS OF LITHIUM-DIFFUSION CONSTANT

The first direct measurements of effective lithium-diffusion constant in silicon solar cells were made under Contract NAS5-10239 and reported in Reference 4. The diffusion constant was measured at the edge of the depletion region by measuring the time rate of change in zero-bias capacitance of the cell with the cell under a reverse bias of 3V. In most of the cells tested, the diffusion constant measured was a small fraction of the free lithium-diffusion constant measured by Pell (Reference 22). Diffusion-length recovery measurements on the same cells (Reference 4) lead to the hypothesis that the lithium-diffusion constant increased with distance from the junction edge to a value approximating the free lithium-diffusion constant of 2×10^{-14} cm^2/sec throughout most of the ($\gtrsim 30\,\mu m$ thick) current-collection volume of these cells. In the First Quarterly Report of the present contract a method for extending the diffusion-constant measurement into the base region of the cell was outlined. The experimental method involves the application of a steady reverse bias, V_b, and the measurement of the time rate of change in voltage, dV_a/dt, for a given capacitance obtained initially at a lower reverse bias, V_a. The lithium mobility, μ_{La}, is obtained a distance, $w_a = \epsilon A/C_a$, from the junction through the equation

$$\mu_{La} = \frac{1}{e\xi_a A N_{La}} \frac{dQ}{dt} , \qquad (1)$$

where

ϵ is the permittivity of silicon,

A is the cell area,

C_a is the capacitance at reverse-bias V_a before V_b is applied,

e is the electron charge,

ξ_a is the electric field at w_a due to the bias V_b,

N_{La} is the lithium density at w_a, and

$\frac{dQ}{dt}$ is the time rate of lithium-charge flow across the cell cross-section at w_a.

$\frac{dQ}{dt}$ is found from the equation

$$\frac{dQ}{dt} = \frac{Q}{V} \frac{dV}{dt} , \qquad (2)$$

where

Q is the quantity of charge (electron charge times the integrated donor density) between w = o and w = w_a,

V ($V_{p/n}+V_a$) is the total potential drop across the depletion region for the applied bias V_a, and

$V_{p/n}$ is the junction potential drop at zero bias.

The validity of Eq. (2) depends upon the equation C = dQ/dV reducing to C = Q/αV, where α is a constant. This reduction is valid for either a step junction or a linearly graded junction. Some of the lithium cells have donor-density profiles approximating linear graded junctions. Three of these cells He 867, He 872, and He 887 were chosen for diffusion-constant measurements. Figure 9 gives plots of ΔV_a as a function of time at bias voltage, V_b, for cell He 887. In this cell measurements were taken for three values of V_a, viz., 0V, -1V and -3V. The bias voltage, V_b, was -7V. The curves are linear to a good approximation for small values of ΔV, i.e., small changes in donor-density distribution. The value dV/dt in Eq. (2) is obtained from the slope of these curves. In Figure 9, dV_o/dt is 8×10^{-4} V/min, dV_1/dt is 1.8×10^{-3} V/min, and dV_3/dt is 2.2×10^{-3} V/min. The other quantities in Eqs. (1) and (2), i.e., Q, ξ_a, and N_{La} are obtained from the donor-density profile. The lithium mobility and diffusion constant are thereby obtained as a function of distance, w_a, from the junction. Table VI gives the values of lithium-diffusion constant, D_{La}, (calculated from the lithium mobility by the Einstein relation) at three different values of w_a for each of the three cells tested. The diffusion constant obtained at $V_a = 0$ is that at the edge of the depletion region. It is seen that in each of the cells the diffusion constant is smallest at the depletion region edge and that in two of the three cells the diffusion constant increases monotonically with distance from the junction as had been hypothesized. It should be stated that the error in these measurements could be quite large since the donor-density profile is not strictly linear as was assumed in writing Eq. (2), and since donor-density variations are probably present at a given distance, w, from the junction. However, it is felt that these are less than ±30 percent; consequently, the measurements confirm the hypothesis of lowering of the lithium-diffusion constant near the junction. The lowering of the lithium-diffusion constant is an important factor in cell stability and will be studied further.

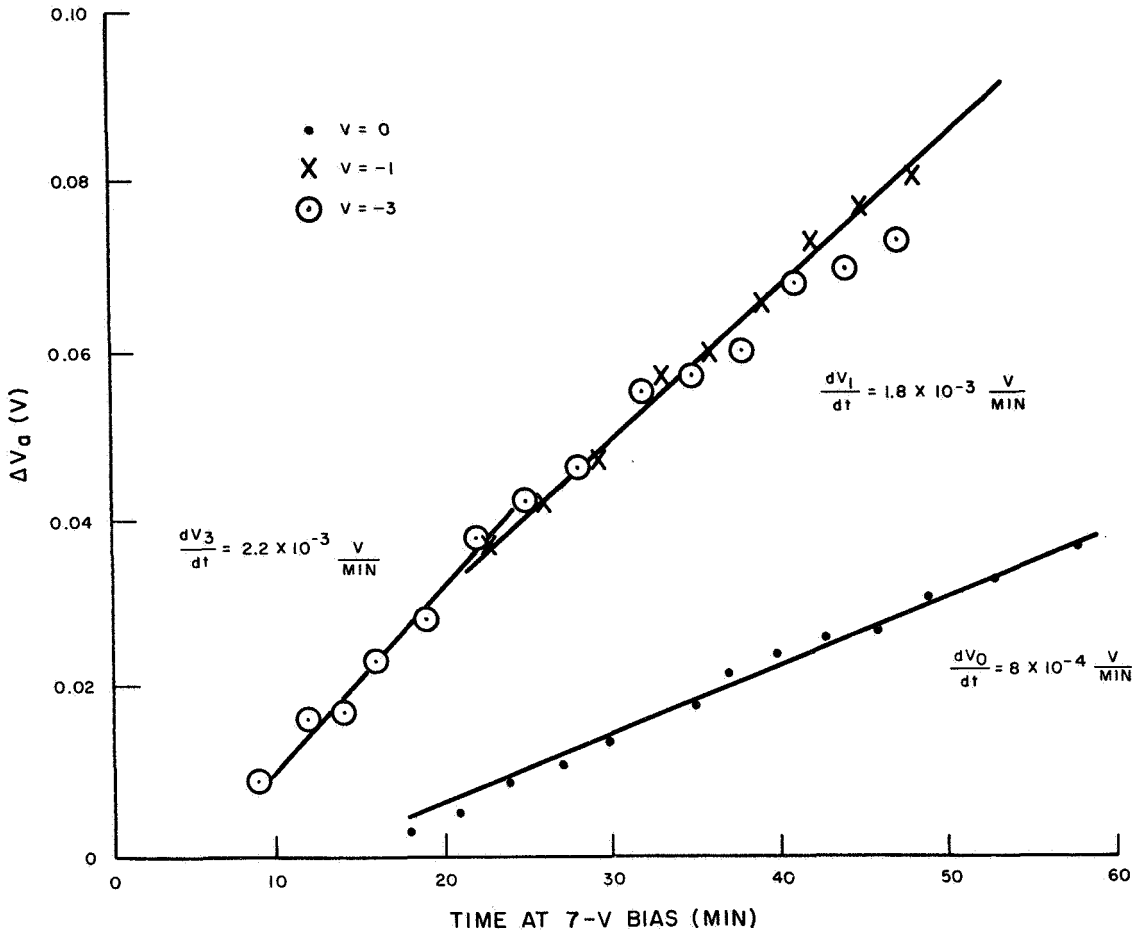

Figure 9. Plots of Change of ΔV_a Versus Time

TABLE VI.

LITHIUM-DIFFUSION CONSTANT AT VARIOUS DISTANCES FROM CELL JUNCTION

Cell	V_a (Volts)	w_a (μm)	D_{La} $cm^2/sec \times 10^{15}$
He 867	0	1.30	3.9
(V_b = -10V)	-2	2.30	6.5
	-5	3.05	>8.5
He 872	0	1.24	3.3
(V_b = -8V)	-2	2.12	9.5
	-4	2.58	5.6
He 887	0	1.35	3.9
(V_b = -7V)	-1	2.00	4.8
	-3	2.75	6.8

SECTION V

LOW-TEMPERATURE MEASUREMENTS

Hall-coefficient and resistivity measurements have been used to investigate the crystal-growth and irradiation-temperature dependence of the introduction rate and room-temperature annealing of carrier-removal defects in lithium-doped silicon. These studies are necessary to understand the mechanisms by which primary defects react with lithium. The reaction products (the secondary defects) are formed during the thermal reordering processes which take place after bombardment produces the primary vacancy - interstitial pair. The electrical properties of electron-irradiated silicon at moderate electron energies (E_e = 1 to 2 MeV) are dominated by these secondary defects. In general, impurities are immobile at or below room temperature, but lithium is an impurity which is highly mobile at room temperature. This mobility makes it possible for lithium to diffuse to radiation-induced defect sites. Evidence to date indicated that the interaction of lithium with the defects neutralized the degrading effect of these defects on the electrical properties of silicon solar cells.

In order to guide the production of radiation-resistant cells, it was necessary to know the ideal quantity of lithium required in the base region of the cell, the way in which lithium interacted with phosphorous, oxygen, and radiation-induced vacancies. The best available way of obtaining this information in its least ambiguous form is by studies of the Hall-effect and resistivity in specially prepared bars of silicon. The information obtained from such study is recognized as being vital to the design of semiconductor devices containing lithium such as the solar cell.

The results of Hall-effect and electrical-conductivity measurements on electron-irradiated silicon doped with lithium are presented in an appendix to this report; this is in the form of a complete scientific paper which is being submitted for publication in the near future. Some very important conclusions flowing from this investigation are given in the next section (Section VI-A-5).

SECTION VI

CONCLUSIONS AND FUTURE PLANS

A. CONCLUSIONS

1. General

In this quarter, two major findings have been made. Firstly, Hall measurements of irradiated lithium-doped silicon bars have given data on many of the important characteristic quantities (concentrations, annealing times and energy levels) for the defects involved in the radiation damage and recovery effect in lithium-doped silicon. The recently-developed capacitance measurement and analysis techniques, used on redegrading lithium cells, have shown that certain characteristics of the lithium concentration profiles in the cells appear to correlate with the tendency of cells to redegrade. The properties which characterize a stable cell can also be discerned.

2. Stability

Long-term stability tests on lithium-doped p/n silicon solar cells irradiated by 1-MeV electrons to fluences from 10^{14} to 10^{16} e/cm^2 indicate that cells made from low-oxygen-content (Lopex or Float-Zone) silicon are more likely to remain stable after recovery for radiation damage if the lithium-density concentration is sufficiently low to avoid significant lithium movement in the region near the junction. Several lithium cells which redegrade after irradiation to 10^{14} e/cm^2, and one which degrades spontaneously with no irradiation display post - degradation photovoltaic characteristics which are not explainable in terms of straightforward solar-cell equivalent circuits. In most redegrading cells, the short-circuit current shows no sensible redegradation during power and open-circuit voltage redegradation. Minority-carrier diffusion length is also relatively constant during redegradation. Thus a short-circuit current measurement does not, in general, provide a sufficient stability criterion in lithium-doped cells.

In Float-Zone silicon cells with moderate lithium density and density-gradient (density $\leq 1 \times 10^{15}$ cm^{-3} at ≈ 1 μm from the junction, density gradient $< 1 \times 10^{19}$ cm^{-4} near the junction) stability in photovoltaic characteristic has been maintained for a period of $\approx$200 days after recovery from 10^{14} e/cm^2. Unirradiated cells with these densities also maintained stable photovoltaic characteristics over an $\approx$11 month period.

3. JPL-Furnished Cells

Photovoltaic measurements and reverse-bias capacitance measurements on the first lot of 20 JPL-furnished cells show that ten Quartz-Crucible silicon cells with low lithium density and density gradient (C1-series) have higher average efficiency under tungsten illumination (10.9 percent) than ten Quartz-Crucible silicon cells (H1-series) with higher lithium density and density gradient (7.5 percent).

4. Lithium-Diffusion Constant

Preliminary measurements of the diffusion constant of lithium at varying distances from the junction in Float-Zone cells generally indicate that this diffusion constant increases with increasing distance from the junction. This supports the previously-proposed hypothesis that the diffusion of lithium is frequently reduced near the junction. Such a reduction, achieved in a controlled manner, should contribute to the stability of lithium cells.

5. Hall Measurements

Silicon Hall bars of two types of crystal growth and two lithium concentrations were bombarded at about twenty controlled temperature (T_B) levels between liquid - nitrogen (79°K) and 280°K. At all temperatures, carrier-removal rates ($\Delta n/\Delta \phi$) were lower than for Stein's comparable irradiations of phosphorus-doped silicon. The difference was greatest at the low temperatures. Introduction rates of carrier-removal defects were exponentially dependent on the reciprocal of bombardment temperature for both types of crystal growth, but the slopes and limiting temperature values differed. The temperature dependence is not consistent with a simple charge-state-dependent probability of interstitial-vacancy dissociation and impurity-vacancy trapping.

Following bombardment, the temperature dependence of the carrier concentration and carrier mobility in the lithium-doped samples was measured periodically in the conventional manner. A characteristic pattern of reappearance of carriers (annealing of carrier removal) and disappearance of charged scattering centers (annealing of mobility) was observed in Float-Zone refined silicon at room temperature. Such recoveries did not occur so strongly in crucible-grown silicon and a different pattern of recovery was observed in this oxygen-rich material.

It is thus clear that some processes specific to lithium as a dopant are being observed. In silicon doped with phosphorus, arsenic, boron etc., there is no similar change of carrier concentration and mobility with time at room temperature. It is very likely, although not proven, that the interactions seen in majority-carrier removal centers are the same as those observed in recovery of minority-carrier lifetime. The most simple scheme of species involved is indicated in Table VII.

TABLE VII.

TENTATIVE ASSIGNMENTS FROM DEFECT SPECIES FORMED IN IRRADIATED LITHIUM-CONTAINING SILICON

Impurity	E_r	First Complex with V^- (Damage Center)	E_r (eV)	Second Complex (Recovered Damage Center After Room Temp. Annealing)	E_r (eV)
Li^+	0.0328	$Li\text{-}V^-$	~0.6*	Li-V-Li	
$Li\text{-}O^+$	0.0394	$LiOV^-$		Li-O-V-Li	
O		OV^- (A-center)	0.186	Li-O-V-Li	
				(OV) (LiOV Li) (Interaction Center)	0.085*
P^+		PV^- (E-center)	0.4	P-V-Li	

* Tentative Assignments

B. FUTURE PLANS

1. Stability Tests

Continuing evaluations will be made on both irradiated and unirradiated solar cells furnished under the previous NASA contract. Lithium cells furnished by JPL under the present contract will be irradiated and monitored for stability and recovery of electrical parameters. Tests will include tungsten photovoltaic measurements, electron-voltaic diffusion-length measurements, 3-color filter wheel measurements, dark current-voltage measurements, and reverse-bias capacitance measurements.

2. Lithium-Diffusion Constant Measurements

Measurements of lithium-diffusion constant as a function of distance from the junction will be continued.

3. Hall and Resistivity Measurements

Hall and resistivity measurements on bulk samples will be continued, although the majority of this effort has been completed.

A surprising feature of the behavior of Float-Zone silicon is the regeneration of donors after the bombardment (see Figure I-3 of Appendix). It was previously thought that, while lithium would be removed during the formation of the second complex or "recovered-damage center" of Table VII, no net change in carrier concentration would occur. The data indicates an unexpected partial dissociation of the first complex (Li-V) which, however, does not occur when oxygen is present.

Results suggest that a lithium-oxygen-vacancy (Li-O-V) complex is produced by electron bombardment in quartz-crucible silicon, and a lithium-vacancy (Li-V) complex in zone-refined silicon. The mechanism of room-temperature annealing is attributed to neutralization of carrier-removal defects by lithium interaction in crucible silicon, and by both lithium interaction and defect dissociation in zone silicon. The Li-V defect is loosely bound compared to the oxygen containing Li O-V defect.

Thus, to fit the above new evidence, the simple schemes of damage and recovery, which were proposed in previous reports require only slight modification, as follows:

Float-Zone Silicon

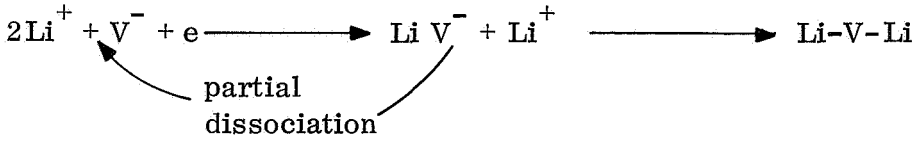

First Complex	Second Complex
(Minority-carrier and carrier-removal damage site)	(Damage recovery site)

Quartz-Crucible Grown Silicon

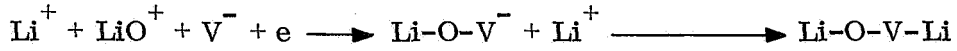

First Complex	Second Complex
(Minority-carrier and carrier-removal damage site)	(Damage recovery site)

Based on the working assumption that the carrier-removal centers observed in this experiment also act as the dominant recombination-centers in irradiated lithium-doped silicon solar cells, several possible mechanisms for the minority-carrier lifetime degradation, annealing, and redegradation processes can be postulated. Thus, it can be postulated that the charged Li OV and Li-V complexes reduce the minority-carrier lifetime. Then lithium atoms complex with radiation-induced

defects, and thereby anneal the initial decrease of minority-carrier lifetime caused by these defects. A second annealing process is the dissociation of defects such as the Li-V complex which does not contain oxygen. The fate of these slowly-generated free vacancies is not known. Lifetime redegradation in the annealed-solar cells could then be attributed to the instability of annealed defect complexes (e.g., Li-V-Li) which do not contain oxygen. In this scheme, the degree of redegradation observed in the post-recovery period of irradiated cells would then depend on the relative number of annealed centers containing oxygen compared to those not containing oxygen.

Further work on analogous experiments involving minority-carrier lifetime measurements will be needed before these models can be confirmed. However, the new evidence of the participation of lithium in slow changes in majority-carrier removal and majority-carrier mobility has put this study of models, for the first time on a firm quantitative basis and, for the first time, indicated the concentrations, charge states, and energy levels of the defects involved.

LIST OF REFERENCES

1. J.J. Wysocki, P. Rappaport, E. Davison, R. Hand, and J.J. Loferski, Appl. Phys. Letters 9, 44 (1966).

2. G.J. Brucker, T. Faith, and A.G. Holmes-Siedle, Final Report on Contract No. NAS5-10239, prepared by RCA and issued March 8, 1968.

3. T.R. Waite, Phys. Rev. 107, 463 (1957).

4. T.J. Faith, G.J. Brucker, A.G. Holmes-Siedle, and R.S. Neadle, IEEE Nuclear and Space Radiations Effects Conf. Missoula, Mont., July 1968, to be published in IEEE Trans. on Nuclear Sci. NS-15 6 (December 1968).

5. G.J. Brucker, T.J. Faith, and A.G. Holmes-Siedle," First Quarterly Report," on JPL Contract No. 952249, prepared by RCA and issued August 15, 1968.

6. W. Rosenzweig, Bell Sys. Tech. Journ. 41, 1573 (1962).

7. (a) D. Kendall and R. Vineyard, NASA Contract No. NAS5-10274.

   (b) P. Payne, G. Goddelle, E.L. Ralph, Heliotek First Periodic Report, NASA Contract No. NAS5-10272, 24 Aug 1966 through 24 Feb 1967.

8. J. Hilibrand and R.D. Gold, RCA Rev. XXI, 245 (1960).

9. J.J. Wysocki, G.J. Brucker, and A.G. Holmes-Siedle, RCA Annual Report, Contract NAS5-10239 (21 June 1966 to 20 June 1967).

10. R.L. Statler, NRL Rept. 6091 USNRL, Washington, D.C. (October 1964).

11. W.R. Cherry and R.L. Statler, GSFC Report X-716-68-204 (April 1968).

12. J.R. Carter, Proc. Sixth Photovoltaic Spec. Conf. IEEE Catalog No. 15C53, Vol. III, 145 (1967).

13. P.H. Fang, Private Communication.

14. P.H. Fang, Proc. Sixth Photovoltaic Spec. Conf. IEEE Catalog No. 15C53, Vol. III, 110, (1967).

15. D. L. Kendall and R. A. Vineyard, Texas Instruments, Inc. Final Report for Contract NAS5-10274, 18 Aug. 66 to 31 Jan. 68.

16. E.M. Pell, Solid State Electronics and Communications, p. 261 Eds. Desirant and Michels, Academic Press, New York (1960).

17. M.B. Prince, J. Appl. Phys., 26, 534, (1955).

18. P. Payne, Heliotek Report No. 11, NASA Contract NAS5-10272, 15 Aug. 1967.

19. M. Wolf and H. Rauschenbach, Adv. Energy Conversion 3, 455 (1963).

20. L. Valdes, Proc. IRE 42, 420 (1954).

21. H.K. Gummel and F.M. Smits, Bell Sys. Tech. Journ., 43, 1103 (1964).

22. E.M. Pell, Phys. Rev. 119, 1222 (1960).

APPENDIX I
ELECTRICAL STUDIES OF ELECTRON-IRRADIATED LITHIUM-CONTAINING N-TYPE Si*

A. INTRODUCTION

Bombardment of silicon crystals by high-energy particles introduces intrinsic defects in the crystal. These defects consist of interstitial-vacancy pairs which are mobile at temperatures as low as 4° K for the interstitial and 75° K for the vacancy (Ref. I-1). Studies of primary defect formation during low-temperature electron bombardment of n-type silicon crystals have been previously reported (Ref. I-2 to I-4). These studies are necessary to understand the production mechanisms of primary defects and their reaction products. The reaction products or secondary defects are formed during the thermal reordering processes which take place after completion of the bombardment. Electrical properties of electron-irradiated silicon at moderate electron energies (E = 1 to 2 MeV) are dominated by the secondary defects formed by the interaction of primary defects with impurities in the crystal. For example, the A-center is a defect-impurity complex consisting of oxygen and a vacancy. In general, impurities are immobile at or below room temperature, but lithium is an impurity which is highly mobile at room temperature. This mobility makes it possible for lithium to diffuse to radiation-induced defect sites. Interaction of lithium with the defects neutralize their degrading effect on the electrical properties of the silicon. However, at a temperature of about 250° K, lithium is virtually "frozen" in the silicon lattice, and the diffusion constant of lithium is reduced to about 1/50 the room temperature value (Ref. I-5). Thus, by irradiating samples at temperatures for which lithium is immobile and then raising the temperature, it is possible to investigate the processes by which lithium interacts with the primary and secondary defects. The information obtained in this study is important in the design of semiconductor devices containing lithium. For example, the power or irradiated-solar cells decreases due to degradation of minority-carrier lifetime. However, it has been shown that electron, neutron, and proton-irradiated-silicon solar cells (Ref. I-6, I-7) containing lithium even when held at room temperature spontaneously recover much of their electrical outputs over a few hours or days following the irradiations. Thus, it appears that the mobile lithium ion moves to, and combines with the original damage center, a vacancy-impurity complex, thereby changing its minority-carrier recombination properties. The resulting new defect complex has a much smaller effect on the minority-carrier lifetime.

* This work was performed under JPL Contract No. 952249 and NASA Contract No. NAS5-10239.

It is the purpose of this paper to report the results of Hall-effect and electrical-conductivity measurements on electron-irradiated silicon doped with lithium. Information concerning the damage mechanisms and properties of carrier-removal defects at bombardment temperatures ranging from 79° K to 280° K will be presented. In addition, the Hall-effect and resistivity measurements were used to monitor the isochronal annealing of defects over a temperature range of 79° K to 250° K. The room-temperature interaction of lithium with carrier-removal defects was monitored as a function of time after irradiation by means of the aforementioned techniques.

This Appendix is divided into four major sections. The experimental techniques, apparatus, types of silicon, and electron source are discussed in paragraph B. The results of carrier-removal and mobility measurements following electron bombardment, and subsequent isochronal and isothermal annealing are presented in paragraph C. These results are discussed in paragraph D with respect to suggested mechanisms of defect formation and annealing, and previous Hall measurements and EPR results that help to identify defects found in lithium-doped silicon.

B. EXPERIMENTAL TECHNIQUES

The Hall-effect and resistivity measurements were obtained by direct current-voltage techniques on Hall bars of 0.3 ohm-cm lithium-doped n-type Quartz-Crucible and Float-Zone silicon. The geometry and dimensions of the Hall bars are shown in Figure I-1a. Thicknesses of samples ranged from 0.016 inch to 0.024 inch. Four samples of each type of crystal growth were used in obtaining carrier-removal production-rates with an average lithium density of 2×10^{16} ±10 percent Li/cm^3 measured at room temperature (297° K) for this group of eight samples. A magnetic field strength of 1600 G and a current of 1 to 3 mA were used to make the measurements. All measurements reported here were made in the dark. The pre-irradiated or post-irradiated samples did not exhibit any significant sensitivity to light. The resistivity of the starting material before diffusion with lithium was 30 ohm-cm phosphorus-doped Quartz-Crucible, and ≥1500 ohm-cm Float-Zone silicon. Lithium diffusion was carried out by heating the starting material in a 1-percent lithium-tin bath at ≈ 400° C for several days. After suitable cleaning processes, the silicon wafers were ultrasonically cut into the shape shown in Figure I-1a. Ohmic contacts were made to the bars by alloying with 1-percent arsenic-tin or 1-percent antimony-gold alloy. Final connection to the alloy dot was made by soldering one end of a fine wire to the dot with indium, and the other end to the indium-tinned gold pattern on a ceramic substrate which provided an insulated base for mounting the samples. The gold pattern was fixed to the ceramic substrate by the standard molybdenum silkscreen process. A thermally conductive epoxy was used to attach the Hall bar to the ceramic substrate. The metallized ceramic substrate was soldered to a copper plate. Six leads of 0.005 inch diameter formvar wire were soldered to the six contacts on the bar and a copper-constantan thermocouple was cemented to one of the arms of the bar as shown in Figure I-1b. The initial impurity concentrations in the Quartz-

Crucible silicon were a phosphorus density of $\approx 1.5 \times 10^{14}$ cm $^{-3}$ and an oxygen density of $\approx 10^{18}$ cm^{-3}. Float-Zone silicon had an oxygen concentration of less than 10^{14} cm^{-3} as determined by the (Li-O) EPR line (Ref. I-8). Thus, the electrical behavior of the irradiated lithium-doped silicon was dominated by oxygen and lithium-defect complexes in crucible-silicon and lithium-defect complexes in zone silicon.

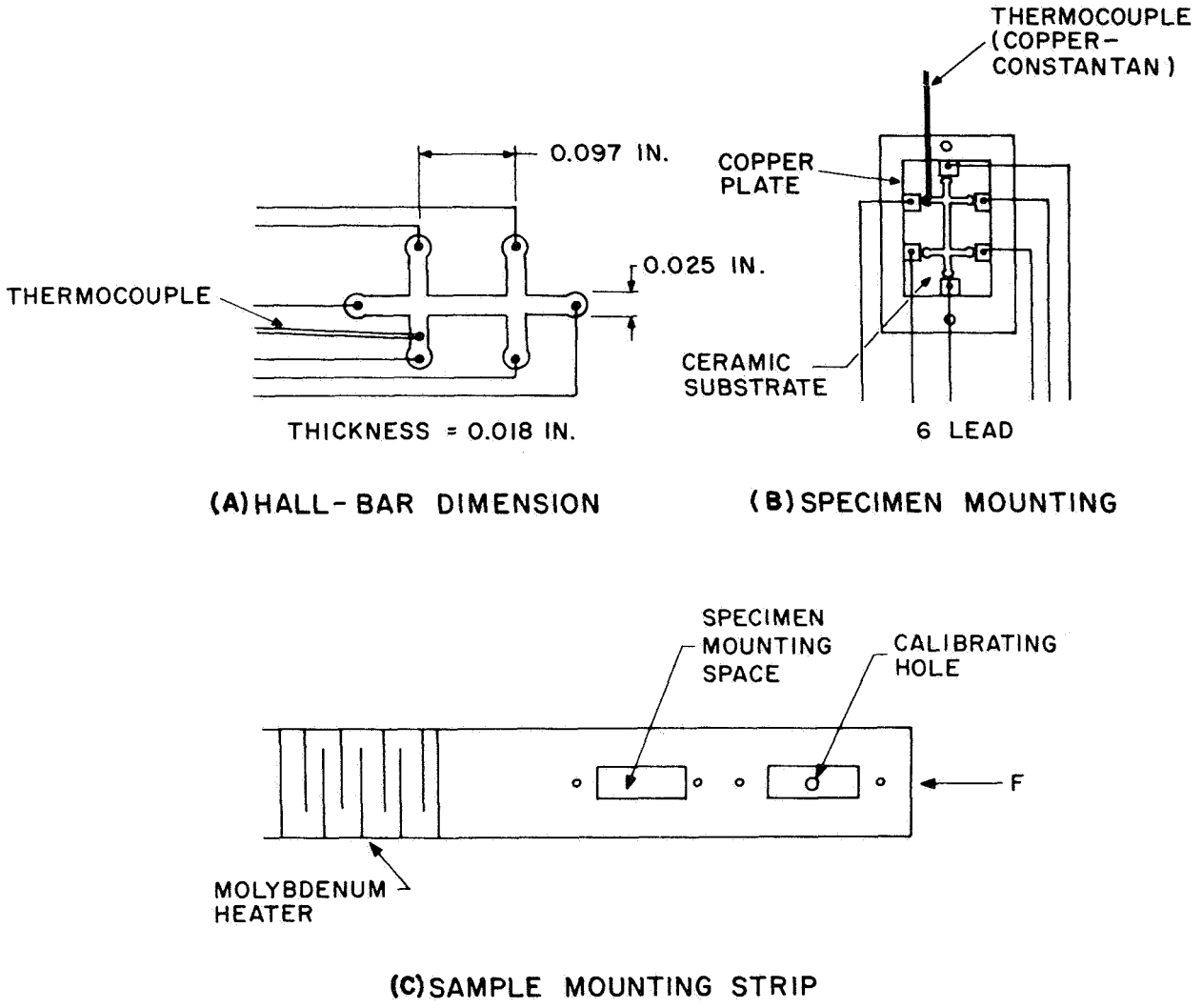

Figure I-1. Sample Geometry and Mounting Configurations: (A) Specimen Shape, (B) Specimen Mounting, and (C) Dewar Finger.

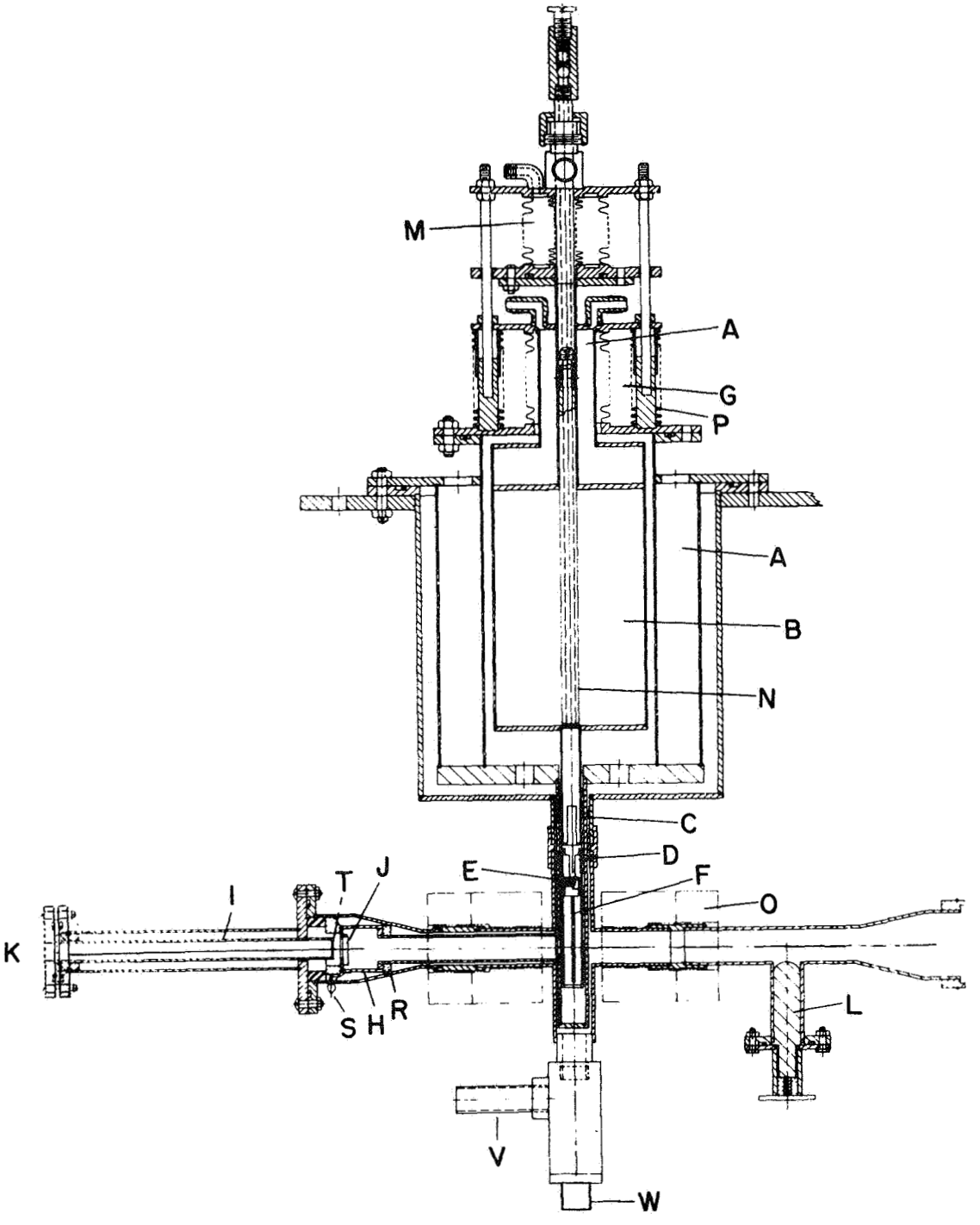

Figure I-2. Irradition and Annealing Apparatus: (A) and (B) Liquid Nitrogen Reservoirs, (C) Dewar finger, (D) Copper Radiation Shield, (E) Molybdenum Heaters, (F) Sample Mounting Strip, (G) Bellows, (H) Faraday Cup, (I) Hollow Tube, (J) Trap Door, (K) Window, (L) Shutter, (M) Bellows, (N) Liquid Nitrogen Filling Tube, (O) Electromagnet, (P) Spring, (R) Lavite Washer, (S) Glass Seal, (T) Phosphor Screen, (U) Electrical Leaks; and (V) Window.

A cross section of the irradiation apparatus is shown in Figure I-2. The principle parts of the apparatus are identified by letters. Section A and B are reservoirs for the liquid nitrogen. The lower portion of the apparatus has two copper radiation shields. One extends down ward from A and the other, D, surrounds the specimen. The sample mounting strip F, shown in detail in Figure I-1c, contains two holes. The specimen is mounted in one and a copper strip with a calibrated hole size, equivalent to the rectangular area which the specimen occupies, is mounted in the other. Either one of these holes can be positioned in the electron beam by means of the double bellows G and spring P. The spring is able to support the structure in its upper position when the space between the bellows is filled with air at atomospheric pressure. When this space is evacuated by a forepump, the bellows contract and lift the inner dewar, and, therefore, the sample holder, to the second position. The system can be cycled rapidly between these two positions by means of an electrically operated valve which alternately exposes the space between the bellows to the atmosphere and to the forepump vacuum. The magnetically operated shutter L is used to interrupt the beam without shutting off the machine, deflecting the beam or disturbing the setup in any way. When the beam is cut off, the sample is dropped into place by activating the three way electrically operated solenoid valve which exposes the bellows M to the air. An electromagnet O, whose axis is concentric with the beam, permits measurements of the Hall coefficient without any disturbance of the sample. The inside of the apparatus is evacuated by means of the vacuum pumping system of the electron accelerator through the opening where the apparatus is jointed to the beam tube.

A 1-MeV Van de Graaff accelerator was used as the electron irradiation source. The electron flux was measured by positioning the Faraday cup H directly behind the space occupied by the hole in F. The cup is insulated by a lavite washer R and has a current lead attached to it via the glass seal S. The uniformity of the beam at the specimen position was checked in the following manner. The beam current was first maximized electrically by adjusting the magnetic lens and the voltage deflection plates. At the "closed" end of the Faraday cup a trap door J was suspended across an opening. A hollow tube I which contained a thin phosphor screen T across one end could be moved through J when a soft iron washer, attached at its opposite end, was moved forward by successively switching on a set of electromagnets wound around in coil form. The phosphor screen was then moved forward until it was directly behind the position reserved for the sample. When the electrons struck the phosphor it fluoresced. The resulting pattern was viewed by a television camera which was positioned behind the window K. Any necessary focusing or deflection was made and then the tube I was withdrawn from the Faraday cup. The trap door J closed and the beam current passing through the hole in F could be measured. The sample leads were brought out of the apparatus through the side arm below the sample as shown in Figure I-2. A quartz glass window W located below the lead feed-through was used to illuminate the sample with band-gap light to check for trapping effects.

The carrier concentration and carrier mobility in the silicon samples were obtained from the Hall-coefficient and the electrical-resistivity measurements. A correction for the ratio of Hall mobility μ_H to conductivity mobility μ_c, was applied to all values of carrier density determined from Hall-coefficient measurements. The ratio μ_H/μ_c was obtained from an empirical equation (Ref. I-4) based on experimental Hall-coefficient data (Ref. I-9).

Samples were sequentially bombarded from the lowest to the highest bombardment temperature in any series of irradiations. The carrier-removal rates measured at the higher bombardment temperatures were determined after larger changes in carrier density had taken place compared to the density changes at the lower irradiation temperatures. Therefore to check the effect of electron fluence on the results, undamaged samples were lightly bombarded at 250° K, and carrier-removal rates determined from the linear region of the carrier density versus fluence curve. The results were in agreement with the carrier-removal rates reported in this paper for this bombardment temperature. However, a sample bombarded to a fluence of 2×10^{17} e/cm^2 exhibited ≈94° percent change in carrier density, and yielded a carrier-removal rate which was smaller by a factor of 5 than the value obtained on the lightly bombarded sample. This fluence dependence of carrier-removal rate occurs for very small (Ref. I-10) or very large values of fluence. To avoid these effects, the samples in this experiment were irradiated to moderate values of electron fluence which resulted in a linear dependence of carrier-density loss on fluence at all bombardment temperatures. After the completion of irradiation at selected bombardment temperatures, measurements of isochronal annealing rates, and the temperature dependence of carrier density and resistivity were made. The annealing temperature was not allowed to exceed 250° K so that the mobility of lithium ions was reduced to 1/50 of the room temperature value. By setting this temperature limit, the interaction of lithium with radiation-induced defects was reduced to a negligible amount. Following the completion of irradiations at all bombardment temperatures, the sample temperature was allowed to increase to room temperature, and the spontaneous interaction of lithium with radiation-induced defects was determined by measurements of the isothermal defect annealing at this temperature of 297° K.

C. EXPERIMENTAL RESULTS

1. Carrier-Removal Rates

Electron irradiation of n-type silicon introduces carrier removal defects which can accept electrons from the conduction band. Thus, carriers are removed from the conduction band and charged-scattering centers are created which reduce the electron mobility. This loss of carriers and reduction of mobility cause the resistivity of the silicon to increase. The effects are separated by measuring both the resistivity and the Hall-coefficient. In these experiments measurements of carrier losses as a function of electron fluence at any bombardment temperature were used to compute a carrier-removal rate $\Delta n/\Delta\Phi$ (CM), and the results for both

crucible and zone silicon are shown in Figure I-3. These removal-rates are those rates which remain after the irradiated samples were annealed to 200° K. Therefore, these rates represent carrier-removal rates of defects which are independent of temperature and have been called ITD defects in previous studies (Ref. I-4). The additional defect which only occures in oxygen-containing silicon at a bombardment temperature of T_B = 250° K produced a peak in the $-\Delta n/\Delta\varphi$ curve for crucible silicon. This defect has been attributed [4] to an oxygen complex since it does not occur in oxygen-lean Float-Zone-grown silicon as indicated in Figure I-3. The curve of $-\Delta n/\Delta\ \phi$ for zone silicon decreases with decreasing temperature at a faster rate than the curve for crucible silicon. Calculations of the slopes of these carrier-removal curves gave 0.09eV and 0.055 eV for the zone and crucible silicon curves, respectively. Apparently the defect-production mechanisms are different in these two types of silicon. Thus, this result suggests that different defects are produced in oxygen-containing silicon compared to oxygen-lean silicon. Carrier-removal rates (Ref. I-4) obtained on crucible and zone silicon doped with phosphorus to 5 x 10^{14} cm^{-3} are also shown in Figure I-3 for comparison. The temperature dependence of $\Delta n/\Delta\phi$ shifted to higher temperatures relative to the results obtained on the phosphorus-doped samples of higher-resistivity. This dependence on resistivity was predicted by the charge-state-dependent theory of Reference I-4. The higher damage rates of the phosphorus-doped samples for both types of silicon are due to the higher energy electrons (E = 1.7 MeV) used to obtain these data, and also to the higher phosphorus-doping density of these samples which cause greater E-center production. It should be noted that the high temperature carrier-removal rate of zone silicon is greater than that of crucible silicon by a factor of $\approx$2.5. A defect complex such as the LiO-V defect is an acceptor which removes two carriers from the conduction band. In a similar way, a Li-V defect will remove two carriers in oxygen-lean silicon. In contrast to this effect, the A-center (OV) removes only a single carrier. Thus, either the production rate of Li-V defects is higher than the LiO-V defect, or more A-centers than LiO-V defects are produced in crucible silicon under the conditions of this experiment. It will be shown later than A-center production appears to be about equal to the LiO-V center production.

Sources of systematic errors in obtaining the carrier-removal rates are primarily: (1) assumed values of μ_H/μ_c for each bombardment temperature, (2) magnetic field measurement in air to represent the value of magnetic field at the sample, (3) the fluence determination, and (4) a measurement or control error of 1° K in bombardment temperature near 80° K means a negligible error in the carrier-removal rate measured in zone silicon and $\approx$15 percent error in crucible silicon based on the measured slopes of 0.09 eV for the zone-silicon and 0.055 eV for the crucible-silicon curves. The last source of error is the dominant one in crucible silicon.

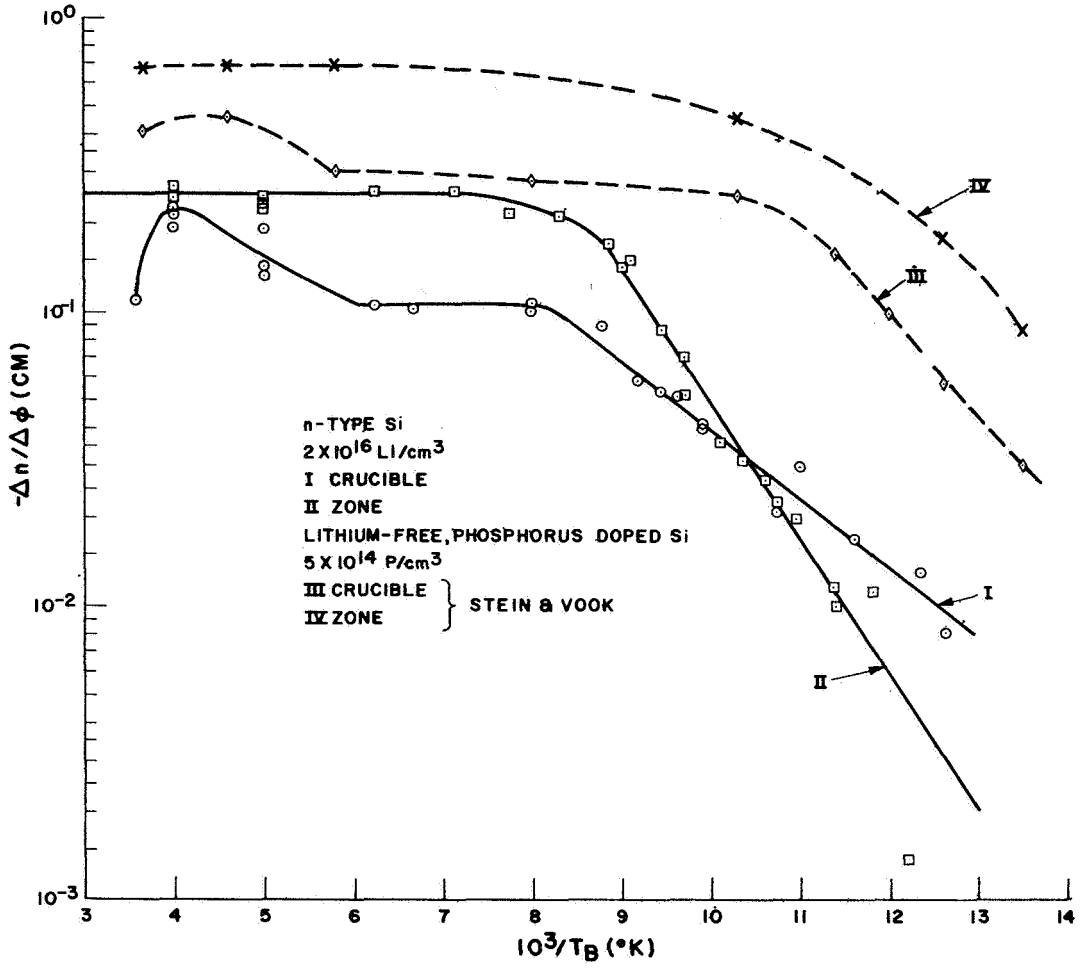

Figure I-3. Carrier-Removal Rates Versus Reciprocal Bombardment Temperature for Float-Zone and Quartz-Crucible Silicon. Measurements at 79° to 81° K after Annealing to 200° K. Results of Stein and Vook (see Ref. I-4) for 10 ohm-cm Phosphorus-Doped Zone and Crucible-Silicon shown for Comparison.

2. Crucible Silicon

a. Carrier-Density Changes

Identification of defects can be accomplished by measuring the carrier density as a function of temperature in order to move the Fermi level through the unknown defect level. Thus, the defect level is filled and emptied of electrons, and

the inflection point in the curve of carrier density versus reciprocal temperature locates the defect-energy level and its concentration. This technique is successful only when the defect level is located between the conduction band and approximately 0.2 eV below the conduction band. Curves of carrier density n, versus reciprocal temperature measured at different times before and after bombardment are shown in Figure I-4. Curve I is the temperature dependence of carrier density immediately after the completion of all bombardments. A defect-energy level located near 0.18 eV is identified as the A-center (Ref. I-2 to I-4). The defect density is about 1×10^{15} cm^{-3} with a temperature T = 220° K at half-filling of the defect level. This A-center concentration is about 1/3 of the total carrier-removal defects calculated from carrier-removal rates and fluences at each bombardment temperature. Since the A-center removes one electron and the LiO-V defect removes two electrons, A-center production appears to be about equal to the LiO-V defect production in the samples of this experiment. Curve III is the temperature dependence of carrier density obtained on the sample after it annealed for 174 hours at 297° K following the completion of bombardment. A spontaneous decrease of carrier density at high temperature, and a slight increase of carrier density at low temperature occurred. The decrease of n at room temperature can be attributed either to the formation of additional deep-lying acceptor levels and/or to loss of lithium due to the complexing of lithium with A-centers or LiO-V-enters. The increase of carrier density at low temperature indicates that acceptors were neutralized. This latter possibility of a lithium loss to explain the decrease of carrier denisty at high temperature is strongly supported by the increase of the Hall mobility at low temperature. The defect center previously located near 0.18 eV shifted to 0.16 eV below the conduction band. A new level located near E_c -0.08 eV is indicated by Curve III. This level also appears in irradiated-crucible silicon of low-doping density (2×10^{15} cm^{-3}) after annealing to 297° K, but the level appeared to be very distinct and measurable (see Figure I-10). The final curve shown in Figure I-4 was obtained after annealing for 10 minutes at a temperature of 373° K. The purpose of this technique was to speed up the interaction of lithium with radiation-induced defects. Curve IV shows that all defect levels have disappeared and the carrier density has decreased extensively at all temperatures. Thus, the interaction time of lithium with defects was accelerated considerably by the high temperature annealing. All defects appear to be neutralized at an annealing temperature and for a duration which is insufficient to anneal normal defect centers (e.g., A, E, C, etc.).

b. Mobility Changes

The Hall-mobility data gives strong support to the suggested annealing mechanism of lithium complexing with defects and neutralizing their electrical effect. Figure I-5 shows the Hall-mobility versus reciprocal temperature for the same sample and measured under the same conditions as in Figure I-4. Curve II is the mobility measured immediately after bombardment. Curves III and IV show the

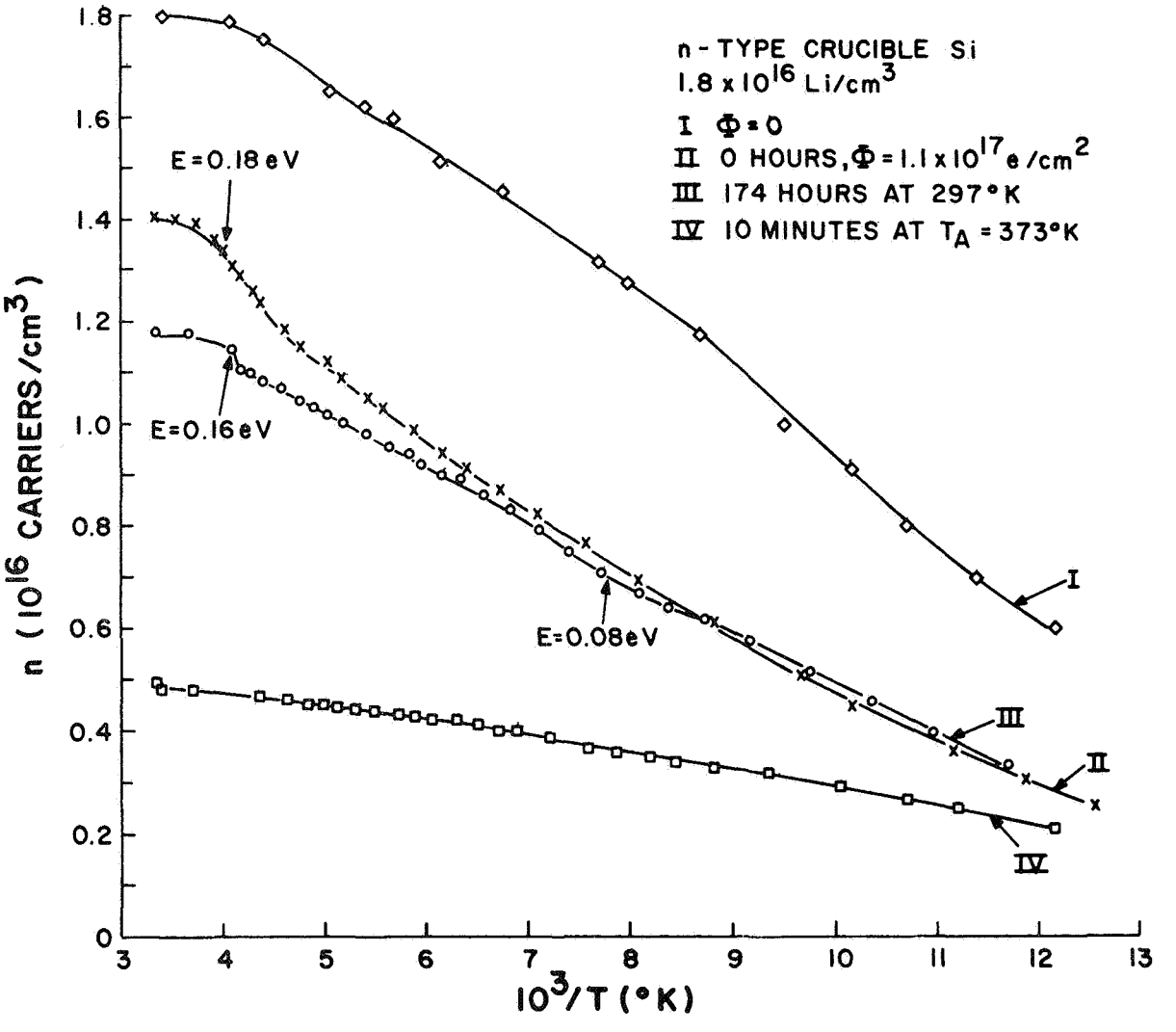

Figure I-4. Carrier Density Versus Reciprocal Temperature for Crucible Silicon (1) Before Irradiation, (2) Immediately after Irradiation, (3) Annealing to a Temperature of 297°K for 174 hours, and (4) Then Annealing for 10 min. at a temperature of 373°K.

mobility progressively recovering from the state of damage after 34 and 174 hours at 297°K following bombardment. Clearly, charged-scattering centers are being neutralized since the mobility varies inversely with the number of charged centers. Curve V is the mobility measured after the sample was annealed for 10 minutes at a temperature of 373°K. These measurements showed that the mobility completely recovered to approximately the pre-irradiation values. Therefore, the scattering conditions in the sample after this annealing process are equivalent to the initial conditions before bombardment.

3. Zone Silicon

a. Carrier-Density Changes

In order to study the effect of oxygen on the results, samples fabricated from Float-Zone Silicon were irradiated and measured. The low-oxygen content ($\leq 10^{14}$ cm^{-3}) and high resistivity ($\geq$ 1500 ohm-cm) of the starting silicon prevented a significant number of impurity-defect complexes from forming except for lithium-defect complexes. Figure I-6 shows the carrier density versus reciprocal temperature measured before bombardment, immediately following bombardment, and after 17 hours at room temperature following bombardment. Irradiated float-zone silicon exhibited an increase of carrier density at all temperatures, instead of a spontaneous decrease of carrier density which occurred in crucible silicon after annealing at room temperature. Both mechanisms of dissociation of carrier-removal defects, and neutralization of these defects by lithium takes place in irradiated-float-zone silicon soon after bombardment. Studies of annealing kinetics performed on lithium-doped solar cells (Ref. I-6, I-11) indicate that the mechanism of annealing is an interaction by lithium with recombination-defect centers which neutralize their degrading effect on minority-carrier lifetime. The mechanism of solar cell annealing by the annihilation of a Li-V defect has also been proposed (Ref. I-12). The fast reaction at room temperature is due to the lack of oxygen which combines with lithium and decreases the free-lithium diffusion constant (Ref. I-5) in crucible silicon. For the concentration of lithium and oxygen in the samples used in this experiment, the diffusion constant in crucible silicon is $\approx 1/100$ the diffusion constant of lithium in zone silicon.

b. Mobility Changes

The decrease of the mobility is consistent with the introduction of charged-scattering defects in samples bombarded by electrons Figure I-7 shows the mobility dependence on temperature for the same sample and conditions described in Figure I-6. After the 17 hour annealing period, the mobility completely recovered to slightly better than the initial values. This speed of recovery is to be contrasted with the speed of mobility-recovery in crucible silicon as shown in Figure I-5. Measurements on a crucible-silicon sample annealing at 297° K for 40 days after bombardment still showed that the mobility had not fully recovered. Thus without the necessity of annealing to a temperature of 100° C, irradiated-zone silicon exhibits neutralization and dissociation of all charged scattering centers in $\leq$ 17 hours at room temperature after completion of bombardment.

Recovery of mobility is controlled by the complexing mechanism of annealing if the assumption is made that only one lithium donor is required to neutralize a lithium-defect complex. Thus, there is no effective change in carrier density, but there is a decrease in the number of charge-scattering centers. The increase of carrier

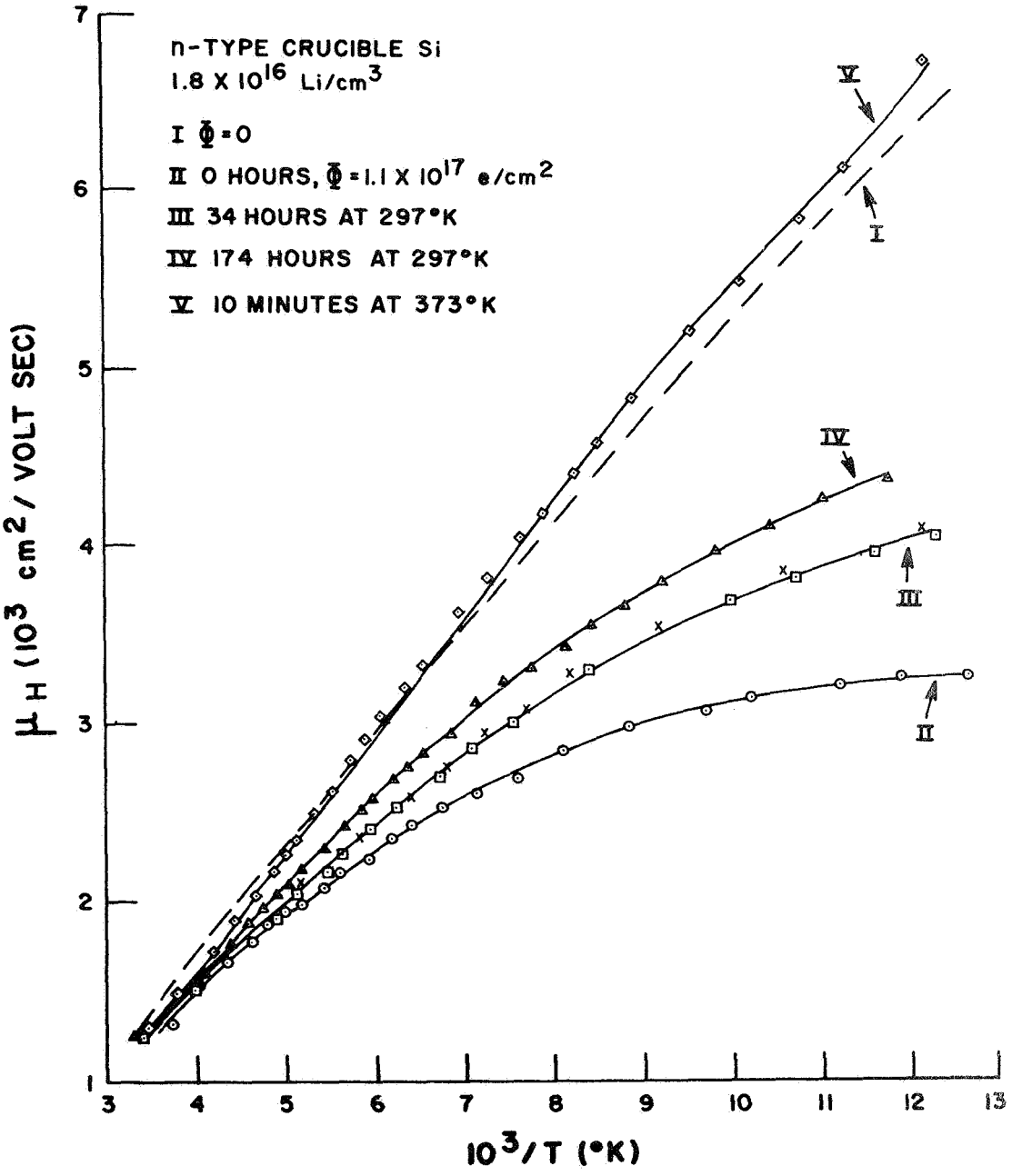

Figure I-5. Hall mobility versus reciprocal temperature for crucible silicon, (1) before irradiation, (2) immediately after irradiation, (3) annealing to a temperature of 297° K for 34 hours, (4) annealing to a temperature of 297° K for 174 hours, and (5) then annealing for 10 min. to a temperature of 373° K.

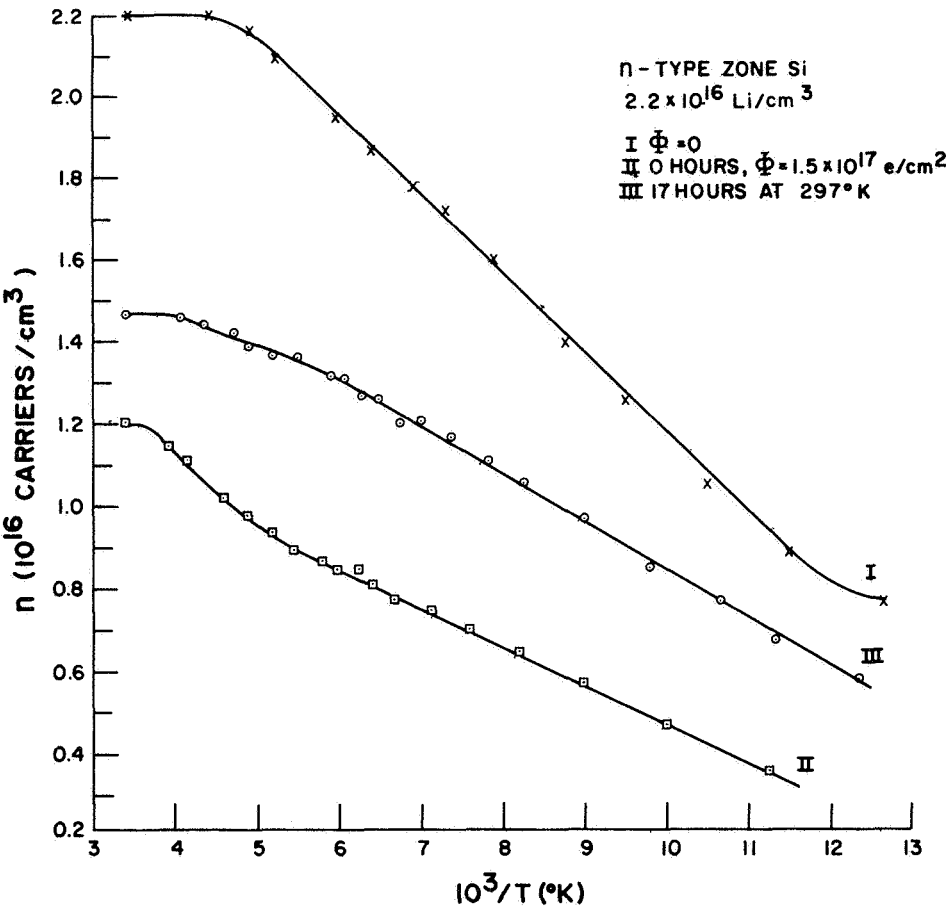

Figure I-6. Carrier density versus reciprocal temperature for zone silicon, (1) before irradiation, (2) immediately after irradiation, and (3) annealing to a temperature of 297° K for 17 hours.

density is controlled by the mechanism of dissocation. Therefore, a measurement of recovery kinetics would indicate the existence of the two processes. Accordingly, a sample of zone silicon was irradiated to a fluence of 2 x 10^{15} e/cm^2 at a bombardment temperature of 250° K, and then isothermally annealed at a temperature of 297° K. Measurements of mobility and carrier density were made at temperatures of 83° K and at 297° K. The results are shown in Figure I-8 where the unannealed fraction of reciprocal mobility f_μ and of carrier density f_n are plotted versus the annealing time. The mobility recovers faster than the carrier density. It appears that recovery from radiation damage by a defect-complexing process and by a defect-dissociation process act in parallel. A surprising result was the additional annealing stage which commenced at an annealing time of 120 min. Measurements made at annealing times of 63 and 255 hours indicated that this second annealing stage was unstable since the mobility and carrier density returned to the recovery levels achieved after the first stage of recovery. The zone-silicon samples used

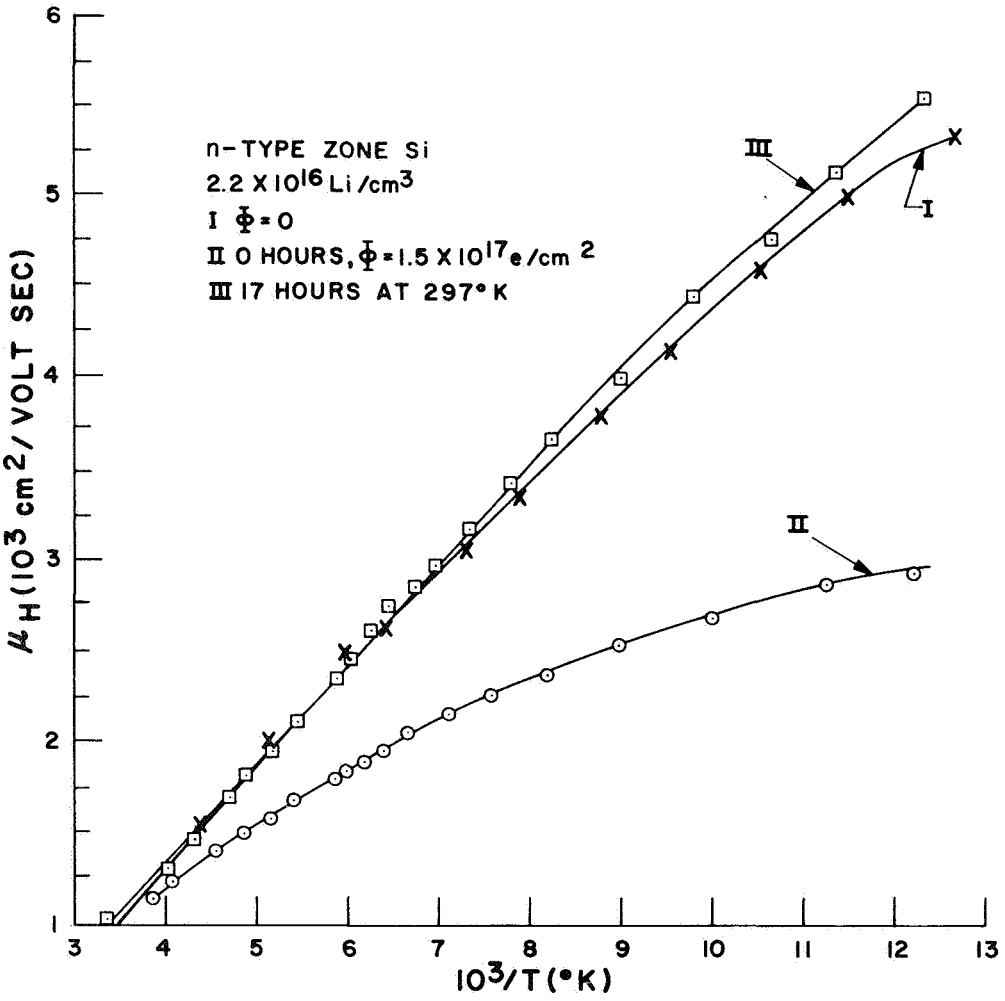

Figure I-7. Hall mobility versus reciprocal temperature for zone silicon, (1) before irradiation, (2) immediately after irradiation, and (3) annealing to a temperature of 297° K for 17 hours.

in obtaining carrier-removal rates were remeasured 79 days after bombardment to check the long-term stability of the annealed samples. They did not show any significant change from the recovered-carrier density and values of mobility indicated in Figures I-6 and I-7. The carrier denisty measured at a temperature of 297° K increased as is shown in Figure I-8. This indicated that the free lithium density increased as a result of Li-V defects dissociating. The mobility measured at 297° K did not change since it is dominated by lattice scattering rather than charged-defect scattering at this temperature.

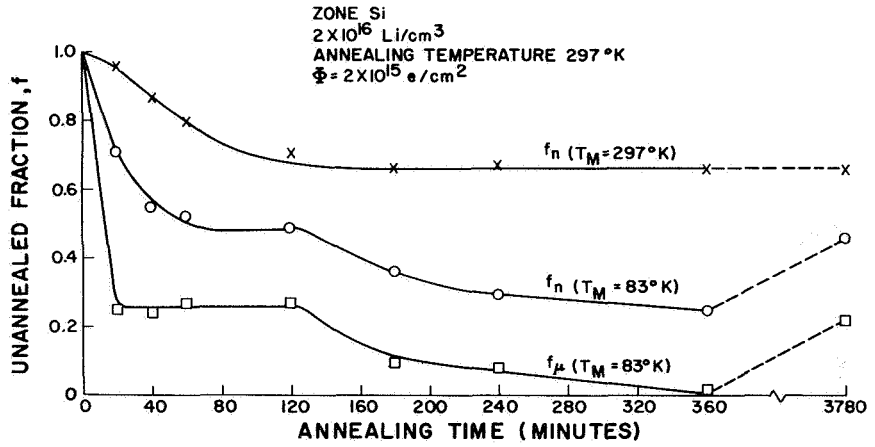

Figure I-8. Unannealed fraction of carrier density f_n and unannealed fraction of reciprocal mobility f_μ versus annealing time. Measurements made at 297° K and 83° K on zone silicon irradiated at 250° K and annealed to a temperature of 297° K

4. High Resistivity Crucible Silicon

a. Annealing

The purpose of this paper was to study the production mechanisms of primary and secondary defects in electron-irradiated silicon containing lithium. The high concentration of oxygen ($10^{18}cm^{-3}$) in crucible silicon prevents the formation of lithium-defect complexes in measurable quantities in samples doped with lithium to concentrations of $\approx 2 \times 10^{15}cm^{-3}$. For this reason, the major portion of the work was carried out on samples doped with lithium to a concentration of $2 \times 10^{16}cm^{-3}$. The production of A-centers dominates in crucible silicon of low doping density. This has been shown in recent EPR measurements (Ref. I-13) and also will be shown in this paper. A sample of crucible silicon from the same 30 ohm-cm material used in all these measurements was doped with lithium to a concentration of $2 \times 10^{15}cm^{-3}$ and irradiated with electrons at bombardment temperatures of 79° K and 250° K.

After the completion of the low-temperature bombardments an isochronal annealing cycle of 10 min duration at each annealing temperature up to a limit of 250°K was carried out. The upper-temperature limit was set at 250° K to prevent lithium motion and interaction with defects from occurring. The product of the unannealed fraction and $-\Delta n/\Delta\Phi$ (cm) is shown in Figure I-9 together with the unannealed fraction of $1/\mu$. There appears to be two annealing stages and a reverse annealing peak at 250° K which has been observed in previous electrical experiments. Following the description of Stein and Vook (Ref. I-4), both stages are attributed to the annealing of ITI

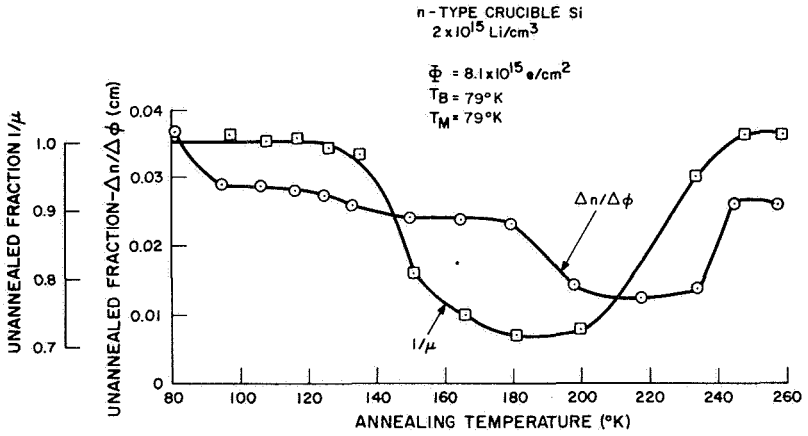

Figure I-9. Unannealed fraction of carrier-removal rate and mobility versus annealing temperature for high resistivity (2.5 ohm-cm) crucible silicon after irradiation at 79°K with measurements at 79°K

(Irradiation-Temperature Independent) defects in the temperature range of 100°K to 200°K. Stein and Vook attributed the reverse annealing peak to the formation of a defect located near an energy of 0.13 eV below the conduction band. This reverse annealing peak is not observed in oxygen-lean Float-Zone silicon, and thus the production of this defect requires the presence of oxygen. The separation of the total carrier-removal rate into the separate defect components can be deduced from the annealing cycle. Thus 0.02 cm^{-1} is attributed to ITI defects, and 0.016 cm^{-1} to ITD defects (Irradiation-Temperature Dependent). The ITD defects are those which involve impurities such as oxygen, phosphorus or lithium. In the present case, the phosphorus background is quite low, ($\approx 10^{14} P/cm^3$), thus E-centers are not expected to occur in significant quantities. The two possibilities are the A-centers (OV) or a center involving lithium. More will be said about this latter possibility in the discussion. Correlation of mobility changes with carrier-density changes during the annealing cycle are indicated in Figure I-9 where the unannealed fraction of $1/\mu$ is plotted versus annealing temperature. The fraction f_μ is given by Equation (1).

$$f_\mu = \frac{1/\mu\,(T) - 1/\mu_o}{1/\mu\,(79°K) - 1/\mu_o} \qquad \text{(I-1)}$$

where $1/\mu\,(T)$ is the reciprocal value of mobility after annealing at temperature T and measured at T = 79°K, $1/\mu\,(79°K)$ is the post-bombardment value of reciprocal mobility measured at 79°K, and $1/\mu_o$ is the pre-bombardment value of reciprocal mobility measured at T = 79°K. The annealing cycle of $1/\mu$ showed only a single stage of annealing, but the reverse annealing peak at T = 250°K was in agreement with the

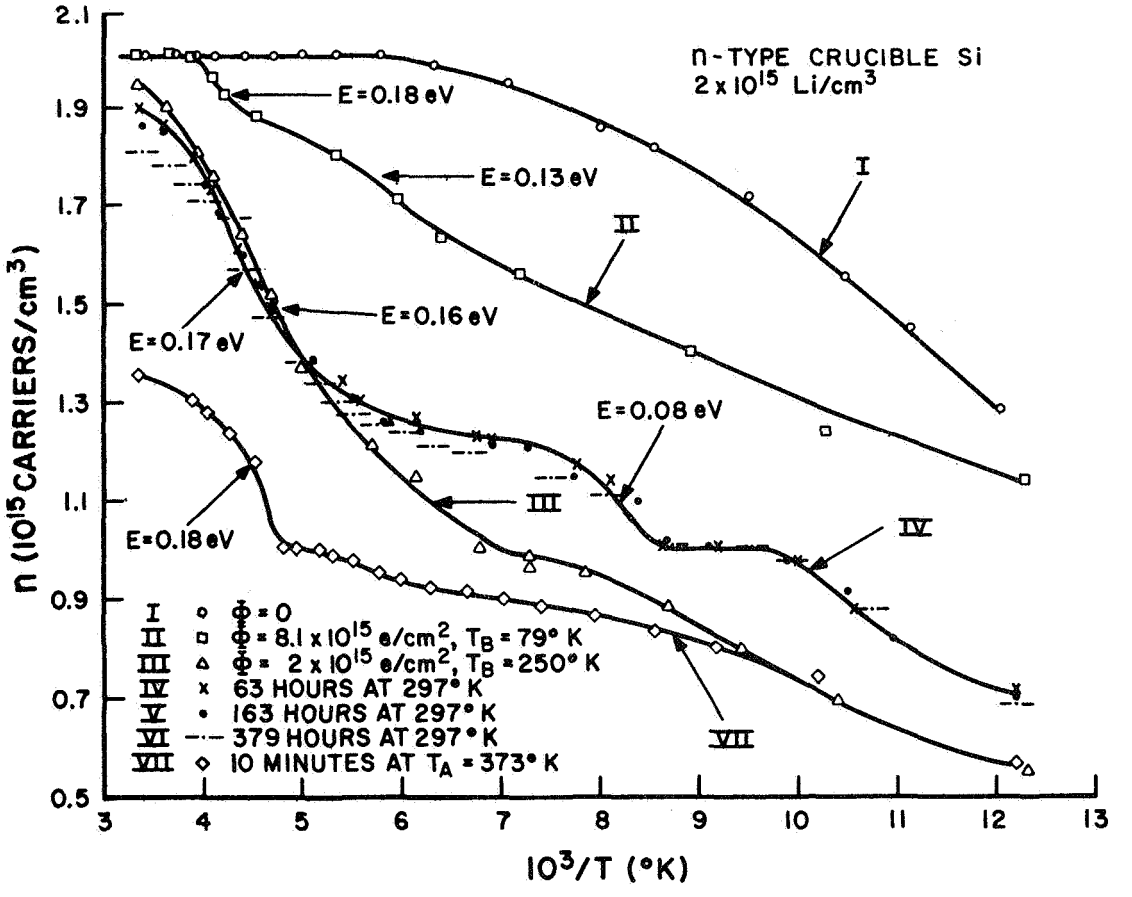

Figure I-10. Carrier-density versus reciprocal temperature for high resistivity (2.5 ohm-cm) crucible silicon, (1) before irradiation, (2) after irradiation at 79°K plus annealing to 250°K, (3) after irradiation at 250°K, (4) annealing to a temperature of 297°K for 63 hours, (5) annealing to a temperature of 297°K for 163 hours, (6) annealing to a temperature of 297°K for 379 hours, and (7) annealing to 373°K for 10 min.

annealing cycle of the carrier-removal rate. The annealing curve agrees qualitatively with the results obtained on phosphorus-doped crucible silicon (Ref. I-4) of 10 ohm-cm resistivity, and also on lithium-doped crucible silicon of 0.3 ohm-cm. The qualitative results are independent of the dopants and their densities in these samples.

b. Carrier Density Changes

The remaining results are concerned with the temperature dependence of carrier density measured immediately after each irradiation, and then as a function of time after the last irradiation with the sample annealing at room temperature. These data are shown in Figure I-10. The most interesting results in the data of

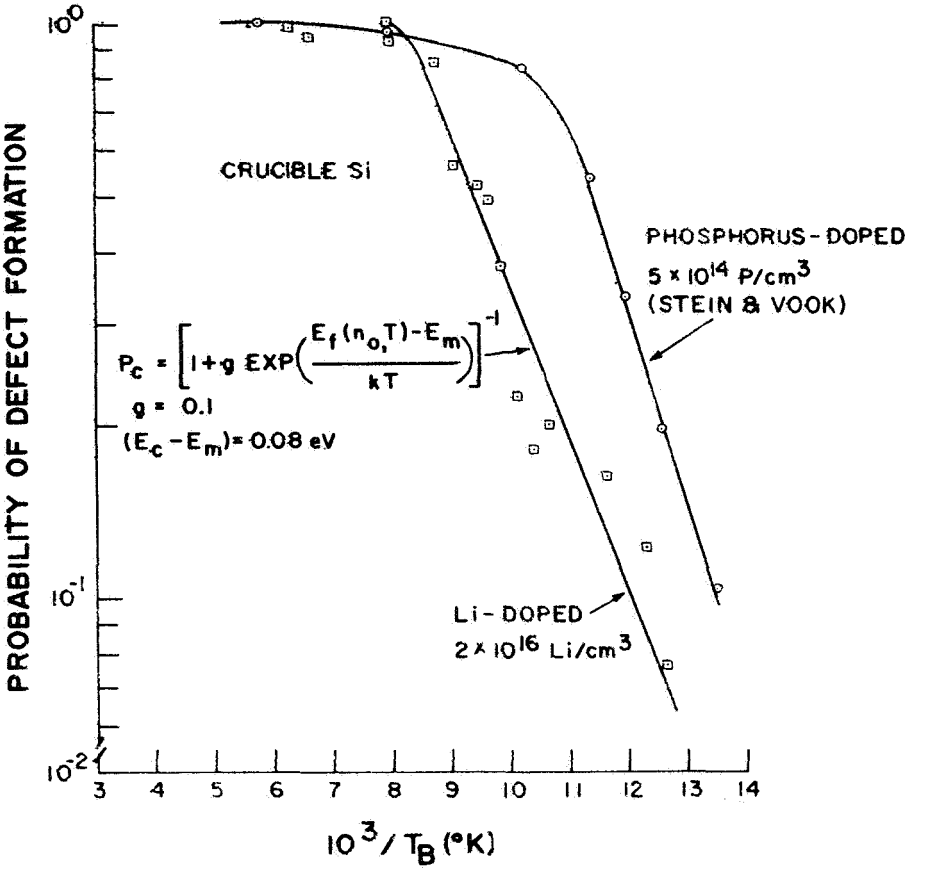

Figure I-11. Comparison of predicted defect-production probability for the charge state-limited model with measurements of defect production rates for crucible silicon. Experimental and calculated values have been normalized. Results of Stein and Vook (see Ref. 4) are shown for comparison.

Figure I-10 are the interaction of lithium with the radiation-induced defects as demonstrated by the temporal behavior of n during the annealing process at room temperature, and the location of defect-energy levels in the carrier-density versus temperature curves. The location of defect-energy-levels can be determined from the curves of n versus reciprocal temperature. The temperature at which half filling of the defect level occurs is indicated in Figure I-10. It can be seen that two energy levels are indicated by curve II which is the data taken after completion of the annealing cycle following the irradiation at a temperature of $T_B = 79°K$. These levels were determined to be 0.18 eV and 0.13 eV below the conduction band which are in agreement with the results of Vook and Stein, namely 0.185 eV and 0.13 eV. The data of curve III for $T_B = 250°K$ in Figure I-10 indicates an energy level extending over a broad temperature range with an approximate temperature $T_{1/2} = 208°K$ for the half-filling of the level. This locates the level at an energy of 0.16 eV below the conduction

band. The determination of the half-filling point is not accurate since the energy of this defect level appears perturbed or smeared out over a broad energy range. Merging of the levels at 0.18 and 0.13 eV would produce a broad energy level such as this one.

Examination of curve IV measured after 63 hours at room temperature following bombardment, shows that the level at 0.17 eV (A-center) is still present, and the 0.13 level has disappeared, however a new level at 0.085 eV has formed. Curve V and VI are measurements taken at t = 163 hrs and 379 hrs after completion of the irradiation. The 0.085 level is still present but significantly the carrier density progressively decreases at high temperature and increases at low temperature.

Loss of carrier density at high temperature and the increase of carrier density at low temperature as a function of annealing time at room temperature is similar to the behavior in the low resistivity (high-doping density) crucible silicon (see Figure I-4). The explanation is the same as the one suggested before, namely lithium complexes with defects to neutralize their electrical effect on carrier density. However, now it is predominantly the A-center which has been affected. The number of LiO-V centers is small and unimportant. Quantitative arguments supporting this idea will be presented in the discussion. Curve VII is the result of annealing the sample at 373°K for 10 minutes, thereby accelerating the interaction of lithium with defect complexes. A defect level approximately located at 0.18 eV and distributed over a wide energy range still remains. The behavior of the mobility substantiated this fact since it did not recover to its initial value as the mobility did in the low resistivity sample. Some residual damage remained even after the high temperature annealing process. The interaction level located at 0.085 eV did not form in Float-Zone silicon and therefore it must require the presence of oxygen for it to occur.

D. DISCUSSION

1. Defect Formation

This study of primary and secondary defect formation during low temperature bombardment by 1-MeV electrons shows that two distinct types of defect dominate the electrical behavior of lithium-doped silicon. The dominant type of defect is a secondary defect formed by the complexing of vacancies with crystal impurities. Vacancies are supplied from metastable interstitial-vacancy close-pairs. The irradiation-temperature dependence of defect formation has been attributed (Ref. I-2, I-4, I-14) to an intrinsic production process of vacancy liberation. This does not appear to be the complete description of defect production mechanisms in lithium-doped silicon. The second type of defect formed during bombardment is introduced at a rate which is independent of irradiation temperature, and this defect is a primary or intrinsic defect as previously reported (Ref. I-4). These defects are called ITI (Irradiation-Temperature-Independent)

defects. Carrier-removal rates shown in Figure I-3 were the results obtained on the samples after annealing to 200°K. The ITI defects anneal between 100°K to 200°K as shown in Figure I-9. The carrier-removal rate of ITI defects was found to be 0.003 ± 002 cm^{-1} in the eight samples of zone and crucible silicon. A value of 0.02 cm^{-1} for the ITI defects was obtained on the high-resistivity sample of crucible silicon. Additional measurements of high resistivity samples are required to confirm this value. Both values of carrier-removal rate due to ITI defects are small compared to the value of 0.075 cm^{-1} reported in Reference I-4. If one adjusts the ITI defect production rates for the higher electron energy (1.7 MeV) used in the experiments of Reference I-4, then the values reported in this paper are still in disagreement by a factor of $\approx$12 for the 0.3 ohm-cm samples. Thus these results suggest a smaller probability of ITI formation in low resistivity lithium-doped silicon.

The irradiation-temperature dependence of the production rate of impurity-complexes in silicon has been explained by a model (Ref. I-2, I-4, I-15) based on the formation of closed-spaced interstitial-vacancy pairs by electron bombardment. This model yields a probability of vacancy liberation from the interstitial to form vacancy-impurity defects. The probability of vacancy liberation from its corresponding interstitial is given by

$$P = \frac{P_c}{1+\gamma \exp E_b^+/kT} + \frac{(1-P_c)}{1+\gamma \exp E_b^-/kT} \qquad \text{(I-2)}$$

where P is the probability of defect formation, γ is the ratio of statistical weights for the jump which annihilates the pair to that which liberates the vacancy from the interstitial, E_b^+ is the energy barrier to liberation when the close-pair is in the more positive state, E_b^- is the energy barrier to liberation when the close-pair is in the more negative state, P_c is the probability of finding the close pair in a metastable state which is more positive, and $(1-P_c)$ is the probability of finding the close pair in a state which is more negative. This probability P_c is given by Equation (3)

$$P_c = \left[1 + g \exp \frac{E_F(n_o, T) - E_M}{kT} \right]^{-1} \qquad \text{(I-3)}$$

where g is the ratio of the number of ways the state can be occupied to the number of ways the state can be unoccupied, $E_F(n_o, T)$ is the Fermi level for electrons which is a function of initial carrier concentration n_o and temperature T, and E_M is the energy level of the metastable interstitial-vacancy pair.

Attempts to fit the data obtained on crucible or zone silicon with the simplified form of Equation (2) where the terms involving the difference in barrier heights are neglected and only the P_c term is considered significant were not completely successful. Data

obtained on 10 ohm-cm phosphorus-doped zone-silicon (Ref. 4) were fitted with Equation (3) and parameters g = 1 and E_M = 0.07 eV were used. The theoretical fit of the data is shown in the normalized defect-production probability curves for crucible silicon in Figure I-11. Equation (3) was used to fit the crucible silicon results of this experiment by setting E_M = 0.08 eV and g = 0.1 and this theoretical curve is also shown in Figure I-11. However, the results obtained on zone silicon cannot be fitted with an expression of this simple form. The normalized probability curves for zone silicon are shown in Figure I-12. The slope of the curve $-\Delta n/\Delta\Phi$ versus reciprocal temperature yields an energy of 0.09 eV. The best fit to the data using the simple charge-state dependent probability of defect formation was obtained with E_M = 0.08 eV and g = 0.013. The theoretical values still disagreed with experimental data in the region of the bend-over temperature. It should be noted that the lithium donor level is located at 0.0328 eV below the conduction band in Float-Zone silicon, and the LiO donor level at .0394 eV

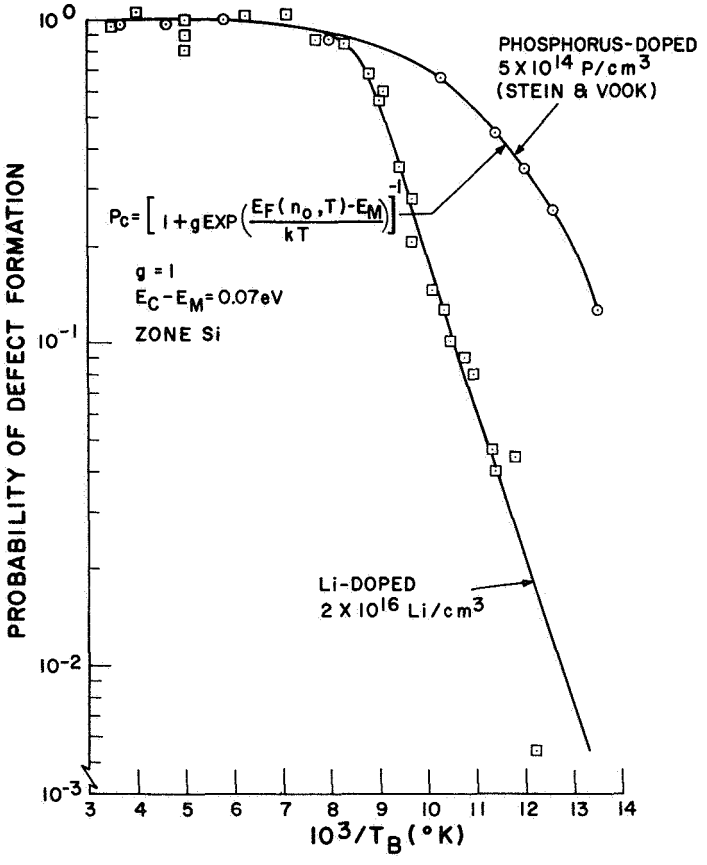

Figure I-12. Comparison of predicted defect-production probability for the charge state-limited model with measurements of defect production rates for zone silicon. Experimental and calculated values have been normalized. Results of Stein and Vook (see Ref. I-4) are shown for comparison.

in crucible silicon (Ref. I-16). This unusual situation means that for the same donor density and temperature, the Fermi level is deeper in the forbidden energy gap in crucible silicon than in zone silicon. Thus at low temperatures, the Fermi filling factor for the metastable-close-pair energy level can be significantly different in the two types of silicon. It appears that either the complete expression given by Equation (2) must be used to fit the data, or the irradiation-temperature dependence does not arise solely from an intrinsic prcduction process. The type of impurity-vacancy complex could play a part in the temperature dependence. However, the results obtained on oxygen containing silicon suggest that an intrinsic process is operative since a good fit of the data with Equation (3) and reasonable values of g and E_M was possible.

2. Defect Annealing

Annealing processes of defects in lithium-doped silicon are unusual since the mobility of lithium makes it possible for lithium to diffuse to and complex with defects at room temperature. High temperatures are not required to anneal large fractions of damage in bulk silicon or devices such as lithium-doped solar cells (Ref. I-6, I-7, I-11). It was shown by the data in Figure I-4 that a temperature of 100°C is sufficient to cause considerable defect annealing. Thus the range of temperatures used to anneal the samples was limited to a range of 79°K to 373°K. In the lower temperature range from 79°K to 250°K, the annealing data obtained on lithium-doped crucible and zone-silicon samples are qualitatively similar to the annealing data obtained on phosphorus-doped silicon (Ref. I-4). Irradiated-crucible and zone silicon exhibited annealing of ITI defects in the temperature range of 100° to 200°K. A reverse annealing peak amounting to a 50-percent increase of carrier-removal rate was observed at 250°K in crucible silicon. The qualitative characteristics of the annealing cycle appear to be independent of impurities other than oxygen. Spontaneous annealing of defects occurred in the irradiated lithium-doped silicon when the samples warmed-up to room temperature. In this respect, the annealing behavior is unique and distinctly different from irradiated-silicon doped with impurities other than lithium. Defect annealing in crucible silicon was clearly demonstrated by the behavior of electron density versus reciprocal temperature shown in Figure I-4 and by the recovery of mobility shown in Figure I-5. It appears that lithium diffuses to and combines with defects to form defect-complexes which are neutral and electrically inactive. The loss of donors at high temperatures is attributed to the loss of LiO donors. The speed of the lithium interaction is slowed down by the oxygen which reduces the free lithium diffusion constant by $\approx 1/100$. Application of heat (100°C) accelerated the interaction of lithium with defects so that complete recovery of mobility occurred. Thus, all radiation-induced charged-scattering centers were neutralized.

In zone silicon the annealing behavior was diametrically opposite to the crucible behavior. Carrier density increased at all temperatures, and the mobility completely recovered within a short period of time at room temperature. It was observed that recovery commenced within an annealing period of 20 minutes at room temperature.

The mechanism of annealing in zone silicon is attributed to lithium complexing with defects and dissociation of loosely bound lithium-vacancy complexes. Both processes act in parallel to anneal radiation damage in zone silicon. However the recovery time constant of the complexing process appears to be faster than the time constant for the process of dissociation.

3. Defect Types and Number

The results indicate that carrier-removal centers are introduced in lithium-doped crucible and zone silicon irradiated by 1-MeV electrons. Identification of the defects responsible for carrier removal can only be inferred from these measurements since this experimental technique is an indirect method, which does not separate out, and examine specific defects as in the more powerful EPR measurement technique. B. Goldstein (Ref. I-13) has observed a four line EPR spectrum in electron-irradiated crucible-silicon, and a single line spectrum in zone-silicon doped with lithium. These damage spectra were attributed to the Li-O-V complex in crucible silicon and the Li-V complex in zone silicon. In those situations where defect energy levels are measurable (e.g., A-center see Figure I-4 and I-10), identification of defects can be made with some degree of certainty with the techniques of this experiment. Defect densities can be obtained from n versus 1/T curves, and compared with values calculated from the measured carrier-removal rates and electron fluences.

The high purity of the Float-Zone samples used in this experiment, minimized the production of E-centers and A-centers. Thus, a Li-V carrier-removal defect-complex appears to be the most probable defect responsible for carrier losses in the zone silicon. In contrast to the zone silicon, the high oxygen concentration in the crucible silicon samples means that oxygen will compete with the LiO donor for vacancies produced by electron bombardment. Lithium complexes readily with oxygen, and at least 70% of the lithium (Ref. I-8) is in the form of LiO immediately after diffusion of the crucible-silicon samples with lithium.

a. High Resistivity Crucible-Grown Silicon

One of the objectives of this investigation was to determine if the lithium-oxygen complex combines with a vacancy to form a defect similar to the E-center. Some limits can be established relative to the possibility of lithium-defect center production by the following considerations. Identification of the defects produced during the irradiations at a temperature of $T_B = 79°K$ in the high-resistivity crucible sample appears sufficiently certain so that an estimated value of lithium-center density can be made. Two energy levels can be seen in curve II of Figure I-9. The one 0.18 eV is close to the value of 0.185 eV below the conduction band reported by Vook and Stein (Ref. I-4), 0.186 eV reported by Novak (Ref. I-3), and 0.183 eV by Wertheim (Ref.

I-17). This defect level is believed to be the A-center. The second defect level in curve II is not as distinct as the A-center. It is located near 0.13 eV which agrees with the value of 0.13 eV obtained in Reference I-4 and attributed to the defect produced during the reverse-annealing peak at an annealing temperature of 250°K.

Based on a carrier-removal rate of $-\Delta n/\Delta\Phi = 0.016$ cm^{-1} plus 0.01 cm^{-1} for the defects produced during the reverse annealing peak, the total number of defects is 2.1×10^{14} cm^{-3}. The total sum of A-centers and the 0.13 eV centers from curve II is 3.6×10^{14} cm^{-3}. Since all the defects calculated on the basis of the carrier-removal rate are accounted for, there does not appear to be any lithium centers produced at $T_B = 79°K$. A further check on this conclusion can be obtained from the change in carrier desnity measured at room temperature after irradiation. If there are no deep centers in the band gap, then the Fermi level corresponding to room temperature should be in a position where all levels are empty and the lithium-donor density is equal to the carrier density. There was no observed loss of lithium measured at room temperature after bombardment at $T_B = 79°K$ as indicated in Figure I-10. The same calculation for the data after irradiation at $T_B = 250°K$ yields 9.5×10^{14} cm^{-3} based on data of curve III in Figure I-10. The identification of these defects is uncertain because of the diffuse nature of this level and the fact that the energy of the level is less than the value for the A-center. However the loss of lithium can be compared to the expected loss based on $-\Delta n/\Delta\Phi = 0.4$ cm^{-1} measured at $T_B = 250°K$. This calculation gives 8×10^{14} defects/cm^3. The observed loss of lithium inferred from the carrier density measured at room temperature was 6×10^{13}Li/cm^3. If lithium forms defect centers at the higher bombardment temperature, then the density is equal to or less than 6×10^{13} defects/cm^3.

After completion of the bombardment, the sample temperature was allowed to increase to 297°K. Two distinct energy levels were observed to occur at 0.17 eV and 0.085 eV below the conduction band, as shown in curve IV and V of Figure I-10. The initial number of defects before interaction by lithium took place was 8 to 9×10^{14} defects/cm^3. Curve IV yields 6.5×10^{14} defects/cm^3 associated with the energy level at 0.17 eV and 2×10^{14} defects associated with the level at 0.085 eV. Thus the total number of defects has not changed after interaction by lithium. The room temperature loss of lithium was 4×10^{13}Li/cm^3.

Curve VII of Figure I-10 shows the carrier density as a function of temperature following the annealing of the sample for 10 minutes to a temperature of 373°K. The total of 8.5×10^{14} cm^{-3} defect centers located at 0.17 eV and 0.085 eV disappeared together with 4.5×10^{14} donors/cm^3 (measured at room temperature) after this annealing process. Approximately 4.6×10^{14} centers/cm^3 located at 0.18 eV remain. Thus, a total of $\approx 4 \times 10^{14}$ defect-centers/cm^3 made up of 2.5×10^{14} A-centers/cm^3 and 2×10^{14} 0.085 eV-centers/cm^3 have been neutralized. The mobility did not recover completely as it did in the low resistivity samples. This is consistent with the residual damage due to the remaining 4.6×10^{14} defects/cm^3. Although the levels are

diffuse and the defect densities are uncertain, the quantitative considerations seem to be consistent with the idea that lithium anneals defects by complexing with them so as to neutralize their electrical effects. If lithium forms defect centers in irradiated low-doping density samples ($\approx 2 \times 10^{15}$ cm^{-3}), then the density of lithium defects after bombardment at $T_B = 250°K$ was less than or equal to 6×10^{13} cm^{-3}. This conclusion is supported by EPR experiments (Ref. I-13) which tentatively identified LiO-V and Li-V damage spectrums in irradiated crucible and zone-silicon samples fabricated from high resistivity silicon and diffused with lithium. The damage spectra were not observed in samples doped with lithium to 2×10^{15} cm^{-3}, but the spectra were observed in the samples doped to densities ranging from 2×10^{16} to 2×10^{17} cm^{-3}.

b. Low Resistivity Crucible Silicon

The total number of carrier removal defects based on the measured $-\Delta n/\Delta\Phi$, and the fluence at each bombardment temperature indicated that 3×10^{15} defects/cm^3 were introduced by the bombardment. Curve II in Figure I-4 shows that $\approx 10^{15}$ A-centers were produced, and a carrier density of $\approx 4 \times 10^{15}$ cm^{-3} measured at room temperature was loss. This implies that $\approx 10^{15}$ lithium defects (LiO-V) were also produced. Curve III indicates that after annealing at room temperature for 174 hrs, a total of $\approx 3 \times 10^{15}$ defects/cm^3 including 2×10^{15} centers/cm^3 located near 0.08 eV remain. This shallow level appears to be the same level observed in the high resistivity sample after annealing at room temperature. However, the level is not as distinct as in the high resistivity sample. The formation of this center required the presence of oxygen and the room-temperature interaction of lithium with carrier-removal centers. The annealing process at 373°K clearly neutralized all defects since the mobility completely recovered. An annealing mechanism which involves the complexing of lithium with defect centers is suggested by these results. All defect centers disappeared after the high temperature annealing. However, residual-defect centers were observed after the same treatment in the high resistivity sample. This latter effect seems to be due to the lower lithium density in this sample.

c. Zone Silicon

Curves of carrier density versus reciprocal temperature shown in Figure I-6 indicate that the energy levels of carrier-removal defects are deep in the forbidden energy gap since moving the Fermi level from close to the conduction band to ≈ 0.2 eV below the band has not revealed any defect levels. The high purity of the initial silicon insures that most of the carrier-removal defects contain lithium. The annealing kinetics of irradiated-zone silicon at room temperature are consistent with the greater lihtium diffusion constant in oxygen-lean silicon. They are also consistent with annealing processes accomplished by lithium complexing with the Li-V defect and by the dissociation of Li-V defects. The dissociation of Li-V defects implies that the

oxygen-containing defects (LiO-V) in crucible silicon are more tightly bound than the Li-V defects in zone silicon (Ref. I-18), since the LiO-V complex appeared to be stable at room temperature within the time period of these measurements. A total carrier loss of 10^{16} cm^{-3} in zone silicon immediately after bombardment is indicated by the data in Figure I-6. Two carriers are removed from the conduction band by each Li-V defect. This means that 5×10^{15} LiV-defects/cm^3 were produced by the bombardment based on the assumption that the Li-V defect is the dominant carrier-removal defect. After the sample annealed at 297°K, the carrier density increased by 2.7×10^{15} cm^{-3}. If it is assumed that the number of dissociated Li-V defects is equal to 1/2 the carrier density increase, then the Li-V defect which did not dissociate is equal to 3.6×10^{15} cm^{-3}. Thus, approximately 28 percent of the carrier-removal defects annealed by dissociation and the remainder annealed by lithium interaction.

d. Mobility Changes

Mobility changes in the irradiated silicon are due to the introduction of charged defects which act as scattering centers. The mobility is proportional to the inverse second power of the charge on the scattering center. Thus, the mobility is quite sensitive to doubly charged defects and large changes in mobility are indicative of mulitply-charged defect centers. The ionized-impurity mobility can be calculated from the Brooks-Herring expression (Ref. I-18) given by

$$\mu_I = \frac{2^{7/2} K^2 (kT)^{3/2}}{\pi^{3/2} (m^*)^{1/2} e^3 N_I \left[\ln(1+b) - b/1+b\right]} \qquad \text{(I-4)}$$

where

$$b = \frac{6K\, m^* (kT)^2}{\pi\, n\, k^2\, e^2} \qquad \text{(I-5)}$$

and K is the dielectric constant of the material, m^* is the density of states effective mass, N_I is the number of ionized impurities, and n is the number of conduction electrons. The total carrier mobility is a combination of the lattice mobility and the ionized-impurity scattering mobility. Expressions have been derived for the relations between lattice, ionized impurity, and conductive mobility. A graph has been computed by Conwell (Ref. I-19) to permit an evaluation of any one of the three if the other two are known. The lattice mobility can be obtained from the work of Logan and Peters (Ref. I-20). Using these procedures, a mobility change was calculated for each zone-silicon sample, and compared to the total-experimental-mobility change. The values of mobility calculated from Equation (4) were consistently lower than the experimental values. Calculated values of the mobility decrease varied from 10 to 25

percent for the four samples. Measured value of the Hall-mobility decrease varied from 20 to 40 percent. Agreement would only be possible if the ratio of Hall mobility to conductivity mobility did not change during irradiation. However, the important point to note is the fact that if the centers were doubly ionized, the calculated mobilities would be considerably smaller than the measured values. This calculation indicated that the Li-V defect is a singly charged defect.

E. ACKNOWLEDGEMENTS

The writer wishes to express his indebtedness to W. Leopold for construction of special circuits and devices, to F. Kolondra who operated the Van de Graaff accelerator, to T. Faith for valuable discussions, R. Neadle who carried out the lithium diffusions, and to D. Liebowitz for fabrication of the samples.

LIST OF REFERENCES FOR APPENDIX I

I-1. G. D. Watkins, Conference Report, Toulouse Conference on Radiation Effects in Semiconductor Components, 1, A1-1 (1967).

I-2. G. K. Wertheim, Phys. Rev. 115, 568 (1959); 110, 1272 (1958).

I-3. R. L. Novak, Ph.D. Thesis, University of Pennsylvania, 1964 (unpublished).

I-4. H. J. Stein and F. L. Vook, Phys. Rev. 163, 790 (1967); "Radiation Effects in Semiconductors," Edited by F. L. Vook. (Plenum Publishing Corporation, New York, 1968) p. 115.

I-5. E. M. Pell, Phys. Rev. 119, 1222 (1960).

I-6. J. J. Wysocki, Proc. Sixth Photovoltaic Spec. Conf., IEEE Catalog No. 15C53, Vol. III, 96 (1967).

I-7. G. J. Brucker and B. Markow, 6th Photovoltaic Spec. Conf. III, 53 (1967).

I-8. B. Goldstein, Phys. Rev. Letters 17, 1 (1966).

I-9. F. J. Morin and J. P. Maita, Phys. Rev. 96, 28 (1954).

I-10. H. J. Stein and R. Gereth, J. Appl. Phys. 39, 2890 (1968).

I-11. T. Faith, G. J. Brucker, A. Holmes-Siedle and R. Neadle, IEEE Trans. on Nuclear Science NS-15, (6), (1968).

I-12. P. H. Fang, "Lattice Defects in Semiconductors," Edited by R. R. Hasiguh, (University of Tokyo Press, Tokyo, 1966) p. 155.

I-13. B. Goldstein, RCA Final Report, Contract No. F19628-68-C-0133 (1968).

I-14. G. D. Watkins, J. Corbett and R. Walker, J. Appl. Phys. 30, 1198 (1959).

I-15. R. E. Whan and F. L. Vook, Phys. Rev. 153, 814 (1967).

I-16. R. L. Aggarwal, P. Fisher, V. Mourzine, and A. K. Ramdas, Phys. Rev. 138, A882, (1965).

I-17. G. K. Wertheim, Phys. Rev., 105, p. 1730 (1957).

I-18. P. P. Debye and E. M. Conwell, Phys. Rev. 93, 693 (1954).

I-19. E. M. Conwell, Proc. IRE 40, 1327 (1952).

I-20. R. A. Logan and A. J. Peters, J. Appl. Phys. 31, 122 (1960).